Geochemistry Geophysics Geosystems G3
AN ELECTRONIC JOURNAL OF THE EARTH SCIENCES
Published by AGU and the Geochemical Society

Article
Volume 9, Number 4
23 April 2008
Q04032, doi:10.1029/2007GC001696
ISSN: 1525-2027

Recent investigations of the 0–5 Ma geomagnetic field recorded by lava flows

C. L. Johnson
Department of Earth and Ocean Sciences, University of British Columbia, 6339 Stores Road, Vancouver, BC, Canada V6T 1Z4 (cjohnson@eos.ubc.ca)

C. G. Constable and L. Tauxe
Scripps Institution of Oceanography, 9500 Gilman Drive, La Jolla, CA 92093, USA (cconstable@ucsd.edu; ltauxe@ucsd.edu)

R. Barendregt
Department of Geography, University of Lethbridge, 4401 University Drive, Lethbridge, Alberta, Canada TIK 3M4 (barendregt@uleth.ca)

L. L. Brown
Department of Geosciences, 611 North Pleasant Street, 233 Morrill Science, Center University of Massachusetts, Amherst, MA 01003-9297, USA (lbrown@geo.umass.edu)

R. S. Coe
Earth and Planetary Sciences Department, University of California, Santa Cruz, CA 95064, USA (rcoe@pmc.ucsc.edu)

P. Layer
Geophysical Institute, 903 Koyukuk Drive, University of Alaska, Fairbanks, AK 99775-7320, USA (player@gi.alaska.edu)

V. Mejia
Universidad Nacional de Colombia, Manizales, Colombia (vmejiab@unal.edu.co)

N. D. Opdyke
Department of Geological Sciences, University of Florida, 241 Williamson Hall, P.O. Box 112120, Gainesville, FL 32611 USA (drno@ufl.edu)

B. S. Singer
Department of Geology and Geophysics, University of Wisconsin-Madison, 1215 West Dayton Street, Madison, WI 53706, USA (bsinger@geology.wisc.edu)

H. Staudigel
Scripps Institution of Oceanography, 9500 Gilman Drive, La Jolla, CA 92093, USA (hstaudigel@ucsd.edu)

D. B. Stone
Geophysical Institute, 903 Koyukuk Drive, University of Alaska, Fairbanks, AK 99775-7320, USA (dstone@gi.alaska.edu)

[1] We present a synthesis of 0–5 Ma paleomagnetic directional data collected from 17 different locations under the collaborative Time Averaged geomagnetic Field Initiative (TAFI). When combined with regional compilations from the northwest United States, the southwest United States, Japan, New Zealand, Hawaii, Mexico, South Pacific, and the Indian Ocean, a data set of over 2000 sites with high quality, stable polarity, and declination and inclination measurements is obtained. This is a more than sevenfold increase over similar quality data in the existing Paleosecular Variation of Recent Lavas (PSVRL) data set, and has greatly improved spatial sampling. The new data set spans 78°S to 53°N, and has sufficient temporal and spatial sampling to allow characterization of latitudinal variations in the time-averaged field (TAF) and paleosecular variation (PSV) for the Brunhes and Matuyama chrons, and for the 0–5 Ma interval combined. The Brunhes and Matuyama chrons exhibit different TAF geometries, notably smaller departures from a geocentric axial dipole field during the Brunhes, consistent with higher dipole strength observed from paleointensity data. Geographical variations in PSV are also different for the Brunhes and Matuyama. Given the high quality of our data set, polarity asymmetries in PSV and the TAF cannot be attributed to viscous overprints, but suggest different underlying field behavior, perhaps related to the influence of long-lived core-mantle boundary conditions on core flow. PSV, as measured by dispersion of virtual geomagnetic poles, shows less latitudinal variation than predicted by current statistical PSV models, or by previous data sets. In particular, the Brunhes data reported here are compatible with a wide range of models, from those that predict constant dispersion as a function of latitude to those that predict an increase in dispersion with latitude. Discriminating among such models could be helped by increased numbers of low-latitude data and new high northern latitude sites. Tests with other data sets, and with simulations, indicate that some of the latitudinal signature previously observed in VGP dispersion can be attributed to the inclusion of low-quality, insufficiently cleaned data with too few samples per site. Our Matuyama data show a stronger dependence of dispersion on latitude than the Brunhes data. The TAF is examined using the variation of inclination anomaly with latitude. Best fit two-parameter models have axial quadrupole contributions of 2–4% of the axial dipole term, and axial octupole contributions of 1–5%. Approximately 2% of the octupole signature is likely the result of bias incurred by averaging unit vectors.

Components: 13,938 words, 14 figures, 13 tables.

Keywords: paleomagnetic; time-averaged field; paleosecular variation; lavas.

Index Terms: 1522 Geomagnetism and Paleomagnetism: Paleomagnetic secular variation; 1545 Geomagnetism and Paleomagnetism: Spatial variations: all harmonics and anomalies; 1599 Geomagnetism and Paleomagnetism: General or miscellaneous.

Received 18 May 2007; **Revised** 8 August 2007; **Accepted** 22 October 2007; **Published** 23 April 2008.

Johnson, C. L., et al. (2008), Recent investigations of the 0–5 Ma geomagnetic field recorded by lava flows, *Geochem. Geophys. Geosyst.*, *9*, Q04032, doi:10.1029/2007GC001696.

1. Introduction

[2] The structure and evolution of the magnetic field is key to understanding the geodynamo and Earth's deep interior, but many aspects of it remain poorly documented particularly on timescales of 10^4 to 10^6 years. While paleomagnetists have made extensive use of the approximation of the time-averaged geomagnetic field by a geocentric axial dipole (GAD), it has been known for some time [*Wilson*, 1970], that there are systematic departures from this simple model. The nature of departures from GAD over the past few million years is debated [*Gubbins and Kelly*, 1993; *Kelly and Gubbins*, 1997; *Johnson and Constable*, 1995, 1997; *Merrill et al.*, 1996; *McElhinny et al.*, 1996; *Carlut and Courtillot*, 1998] (see review given by *Johnson and McFadden* [1997]), and controversy over field structure extends to timescales of 10^8 years and longer [*Piper and Grant*, 1989; *Kent and Smethurst*, 1998; *Van der Voo and Torsvik*, 2001; *Torsvik and Van der Voo*, 2002; *McFadden*, 2004], for which data sets are even sparser in their geographic and temporal sampling. Experiments with the size and nature of the inner core, and with thermal boundary conditions in numerical dynamo simulations [*Hollerbach and Jones*, 1993a, 1993b; *Glatzmaier et al.*, 1999; *Kono and Roberts*, 2002; *Christensen and Olson*, 2003], suggest that non-GAD field structure may

persist over timescales governed by the longevity of the boundary conditions and demonstrate the need to quantify such structure on the basis of measurements of Earth's magnetic field.

[3] Models of the geomagnetic field can be constructed using a spherical harmonic representation. The magnetic scalar potential in a source-free region due to an internal field obeys Laplace's equation, and can be written as

$$\Psi(r,\theta,\phi,t) = a\sum_{l=1}^{\infty}\sum_{m=0}^{l}\left(\frac{a}{r}\right)^{l+1}\left(g_l^m(t)\cos m\phi + h_l^m(t)\sin m\phi\right) \cdot P_l^m(\cos\theta), \quad (1)$$

where $g_l^m(t)$ and $h_l^m(t)$ are the Schmidt partially normalized Gauss coefficients at a time t, a is the radius of the Earth, r, θ and ϕ are radius, colatitude and longitude respectively, and P_l^m are the partially normalized Schmidt functions. The magnetic field, $\vec{B}$, is the gradient of the potential Ψ, and a field model is specified by the Gauss coefficients $g_l^m(t)$ and $h_l^m(t)$. The $m = 0$ terms correspond to spherical harmonic functions with no azimuthal structure; that is, they are axially symmetric or zonal. Here g_1^0, g_2^0, and g_3^0 are the Gauss coefficients representing the axial dipole, axial quadrupole and axial octupole terms, respectively. Time-varying field models can be constructed from time series of magnetic field observations using a parametrization in time (typically cubic b splines). Regularization of models in both time and space minimizes structure that is not required by the data [*Parker*, 1994]. Observatory and satellite measurements provide (B_x, B_y, B_z), the north, east, and downward pointing, locally orthogonal magnetic field components. Paleomagnetic observations are typically measurements of direction (declination (D) and inclination (I)) and/or intensity $|B|$, where

$$D = \tan^{-1}\left(\frac{B_y}{B_x}\right),$$
$$I = \tan^{-1}\left(\frac{B_z}{\left(B_x^2 + B_y^2\right)^{\frac{1}{2}}}\right),$$
$$|B| = \left(B_x^2 + B_y^2 + B_z^2\right)^{1/2}. \quad (2)$$

[4] Over the historical period, 1590–1990 AD, satellite, observatory, and survey measurements of the geomagnetic field have permitted the construction of a spatially detailed, temporally varying magnetic field model, GUFM1 [*Jackson et al.*, 2000; see also, e.g., *Bloxham et al.*, 1989; *Bloxham and Jackson*, 1992]. Starting in the 1970s, similar types of models have also been produced over millenial timescales from compilations of archeomagnetic directional and paleointensity data, and paleomagnetic directional data from high accumulation-rate sediments [e.g., *Hongre et al.*, 1998] (for a review, see *Constable* [2007]); the most recent of these spans the past 7 ka [*Korte and Constable*, 2005]. Time-varying models, such as GUFM1 and CALS7K.2, can be used to examine the evolution of the geomagnetic field. Our interest here is the time-averaged structure: a representation of this is obtained by averaging each of the models over their respective time intervals. The radial component of the magnetic field, B_r, is shown in Figures 1a and 1b for GUFM1 and CALS7K.2, after downward continuation of the scalar potential to the surface of Earth's core under the assumption that the mantle is an insulator. GUFM1 shows significant non-GAD structure, which has been extensively discussed elsewhere [*Jackson et al.*, 2000], and is generally considered to be strongly influenced by the presence of the inner core and the associated tangent cylinder. Regions of increased radial flux at high latitudes, commonly referred to as flux lobes, have persisted in much the same locations for 400 years. Low radial field over the north pole has been interpreted as a manifestation of magnetic thermal winds and polar vortices within the tangent cylinder [*Hulot et al.*, 2002; *Olson and Aurnou*, 1999; *Sreenivasan and Jones*, 2005, 2006]. Equatorial flux patches that are pronounced in the time-varying version of GUFM1 and in modern satellite models [e.g., *Hulot et al.*, 2002], and that appear to propagate westward in the Atlantic hemisphere, are attenuated in the 400 year temporal average (Figure 1a). When averaged over 0–7 ka, CALS7K.2 (Figure 1b) shows longitudinal structure that suggests the presence of flux lobes seen in the historical field. The radial magnetic field is attenuated in CALS7K.2 compared with GUFM1: the resolution and accuracy is clearly inferior, but averaging of millennial-scale secular variation also plays a major role in subduing the structure.

[5] The time interval 0–5 Ma is our primary interest. Three quite different, but representative, field models for this interval are seen in Figures 1c, 1d, and 1e. The simplest one, Figure 1c, is based on the premise that only zonal structure can be resolved, and shows B_r at the core-mantle boundary due to an axial dipole, with a zonal quadrupole contribution, g_2^0, of $0.05g_1^0$. Figures 1d and 1e are constructed using the same techniques of regularized inversion used for GUFM1 and CALS7K.2. These paleofield models are not continuously

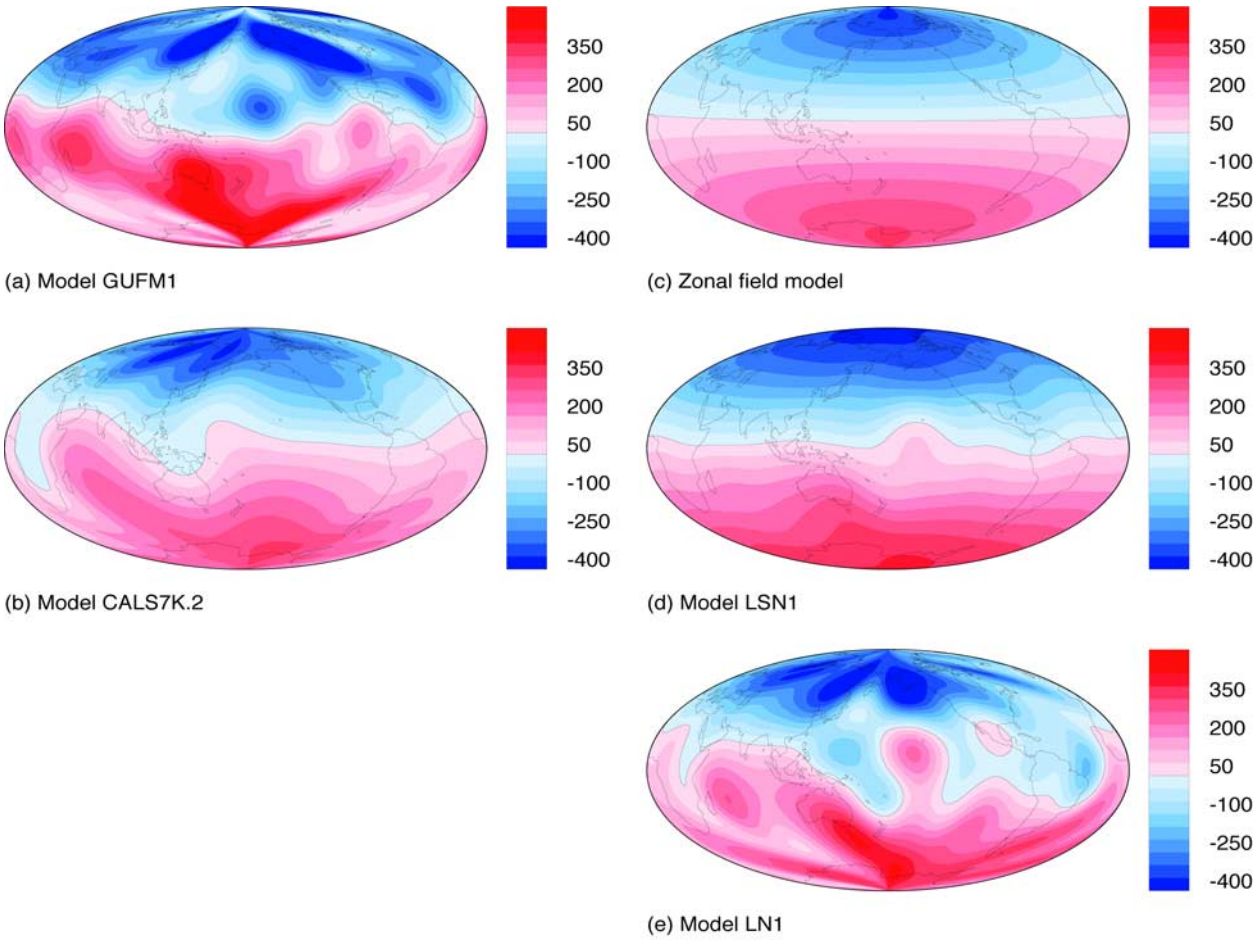

Figure 1. Time-averaged radial magnetic field, (B_r), at the core-mantle boundary (CMB), on different timescales. Units are μT. (a) Historical field: 1590–1990, Model GUFM1 [*Jackson et al.*, 2000], (b) Archeo-Field: 0–7 ka, Model CALS7K.2 [*Korte and Constable*, 2005], (c) Paleo-Field: 0–5 Ma, axial dipole plus axial quadrupole field (see text), (d) Model LSN1 [*Johnson and Constable*, 1997], and (e) Model LN1 [*Johnson and Constable*, 1995].

varying in time, owing to the intermittent record provided by volcanic rocks and the poor spatial data distribution. Instead, time-averaged field directions are inverted for a time-averaged field model (see review by *Johnson and McFadden* [1997]). In Figures 1c–1e, the structure in each model depends on the data sets used: the greatest number of paleodata come from sediment piston cores [*Schneider and Kent*, 1990] with only inclination data and large uncertainties. These are compatible with very smooth models like that shown in Figure 1c. When lava flow observations are combined with sediment data, they suggest the muted nonzonal structure in Figure 1d [*Johnson and Constable*, 1997], and lava flow data alone indicate more complex average field structure (Figure 1e) [*Johnson and Constable*, 1995].

[6] Figure 2 shows the signal expected at Earth's surface for the GUFM1, CALS7K.2 and LSN1 average field models, in the form of geographic variations in departures of inclination and declination from GAD predictions. These are given by the inclination anomaly (ΔI) and declination anomaly (ΔD), where

$$\Delta I = I - I_{GAD} \qquad \Delta D = D. \tag{3}$$

The structure in the archeo and paleofield anomalies is rather similar (despite the very different data distributions from which they are derived) and contrasts with that seen in GUFM1. Note that the magnitude of the signal decreases over longer timescales. From Figure 2f we see that the average inclination anomaly in LSN1 is rather small, and we can expect the largest signal at equatorial latitudes. If this view of the time-averaged field is approximately correct, then at mid to high latitudes it will be difficult to detect departures from GAD without large data sets that provide accurate measures of ΔI.

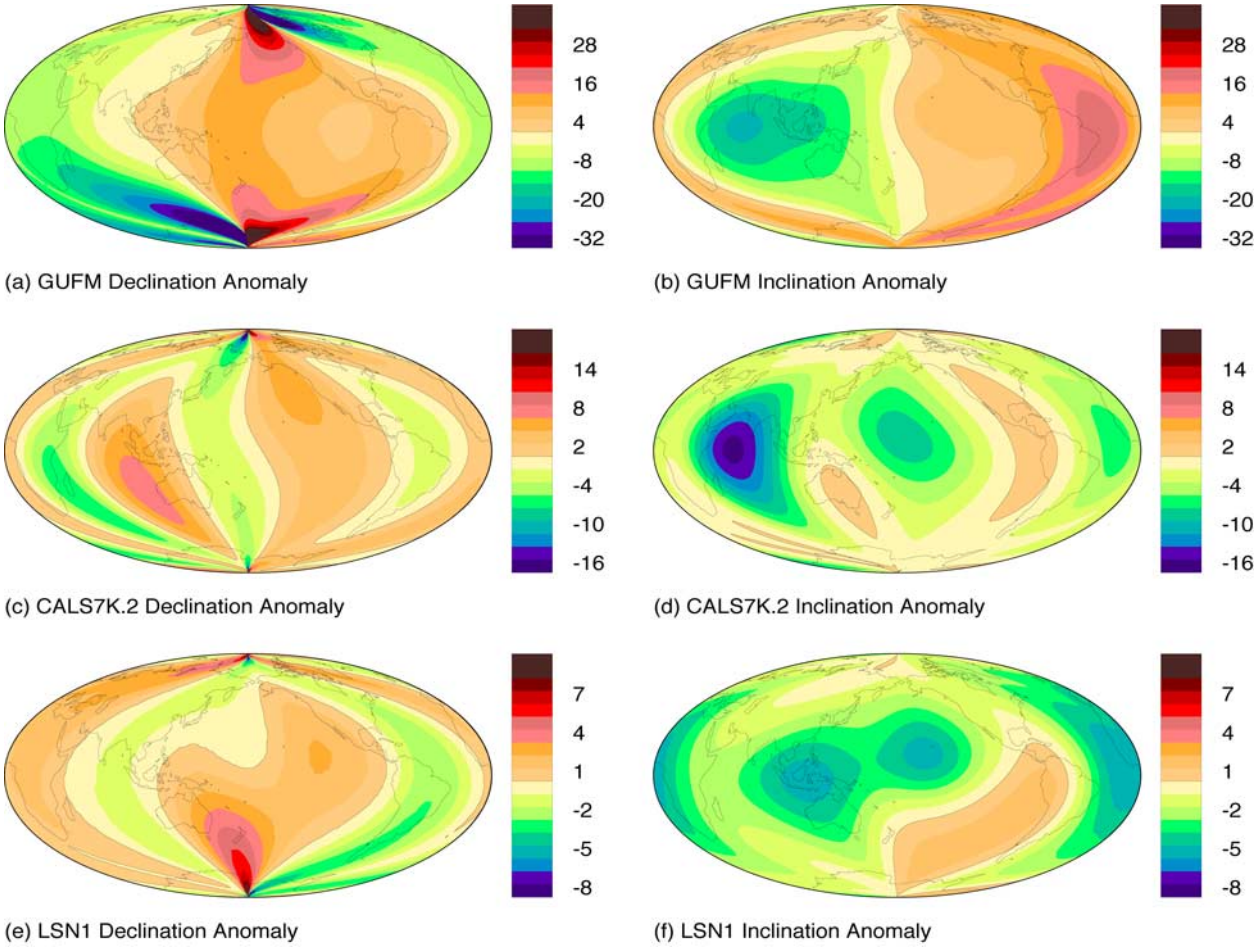

Figure 2. (a, c, e) Declination and (b, d, f) inclination anomalies in degrees (deviations from GAD direction) at Earth's surface predicted from models for the three time intervals in Figure 1: Figures 2a and 2b, Model GUFM1; Figures 2c and 2d, CALS7K.2; and Figures 2e and 2f, Model LSN1. The scale bar for the historical field is twice that for the archeo-field, and 4 times that for paleofield anomalies.

[7] Figures 1 and 2 provide the motivation for gathering the new lava flow data presented here, and for assembling large regional data sets from the published literature. Tantalizing similarities among the models averaged on quite different timescales suggest persistent structure in the time-averaged field in the form of high-latitude flux lobes, and possible low radial field in polar regions. Such structures are not implausible on several grounds. The inner core tangent cylinder might influence core flow in such a way as to produce persistently high values for B_r in the latitude band occupied by the current flux lobes, and lower values close to the pole. It is also possible that these lobes might exhibit longitudinal bias in their locations as a result of geographically complex variations in thermal conditions at the core-mantle boundary. However, the major limitations in understanding geomagnetic field behavior over relevant timescales (10^6 years and longer) are the quality, temporal distribution and spatial coverage of existing paleomagnetic data.

[8] We examine the role of paleomagnetic directions from volcanics in characterizing the 0–5 Ma time-averaged field (TAF) and its temporal variability or paleosecular variation (PSV). We focus on these data for several reasons. First, volcanics provide geologically instantaneous recordings of field behavior, without the temporal averaging inherent in sedimentary records. Second, measurements of absolute declination provide important constraints on longitudinal structure in the field (see discussion by *Johnson and Constable* [1997]), and these are often unavailable from deep sea sediment cores. Third, such data are well-suited to statistical investigations of the paleomagnetic field: they can be used to test the predictions of statistical models such as those pioneered by *Constable and Parker* [1988], the most recent

Table 1. DMAG 4 Data of *McElhinny and McFadden* [1997][a]

Region	*N*	Superseded	Reference
New Zealand	56	yes	this compilation (Table 3)
Japan	21	yes	this compilation (Table 4)
Reunion	27	yes	*Lawrence et al.* [2006]
Tahiti	135	yes	*Lawrence et al.* [2006]
SW USA	54	yes	*Tauxe et al.* [2003]
NW USA	41	yes	*Tauxe et al.* [2004b]
Canaries	13	yes	*Tauxe et al.* [2000]
Iceland	47	no	. . .
Total	394		

[a] These are previously reported data of adequate quality (DMAG 4) for TAF/PSV modeling [*McElhinny and McFadden*, 1997]. N is total number of DMAG 4 data for region (no selection based on k or α_{95}). Superseded indicates whether data from *McElhinny and McFadden* [1997] for that region have been superseded by newer compilations reported by the cited reference. In the case of the SW USA, NW USA, and the Canaries, the recent published data compilations include new data collected as part of the TAFI project.

refinement of which is that of *Tauxe and Kent* [2004]; to compare with the statistical properties of dynamo models [e.g., *Bouligand et al.*, 2005]; or ultimately can be used to invert for both the time-averaged field and its temporal variability (some progress in this area has been made by *Khokhlov et al.* [2001, 2006]). Finally, from a practical perspective, data collection efforts by several groups over the past decade have resulted in many new high-quality paleodirections, that can collectively be compared with those used to generate the models shown in Figures 1 and 2.

[9] In PSV studies of lava flows, an estimate of the paleofield at a given location and time is made by sampling what is known as a "site." At a given site, multiple samples are collected to reduce the influence of measurement error, and these samples must be demagnetized in the laboratory to remove secondary remanence. Site mean values of D and I have an associated uncertainty that reflects within-site scatter. This is usually quoted as the 95% confidence cone about the mean direction, α_{95}, where $\alpha_{95} \approx 140°/\sqrt{kN_s}$ (for k greater than 25) and N_s, k are the number of samples and the estimate of the Fisherian precision parameter, κ respectively. Within-site scatter is sometimes described by the within-site dispersion, s_w, where $s_w = 81°/\sqrt{k}$. Multiple temporally-independent sites are needed to characterize both the TAF and PSV at a single place. A statistic traditionally used to describe PSV is S_B, the root mean square (rms) angular deviation of virtual geomagnetic poles (VGPs) about the geographic axis,

$$S_B = \sqrt{\frac{1}{N-1}\sum_{i=1}^{N}\left(\Delta_i^2 - \frac{S_{w_i}^2}{N_{s_i}}\right)}. \quad (4)$$

Table 2. TAFI Studies[a]

Region	λ, deg	ϕ, deg	N_{total}	N_{dated}	Reference
Aleutians	54.4	190.1	89	31	*Stone and Layer* [2006]
Nunivak	53.0	−172.0	56	0	*Coe et al.* [2000], Appendix A
British Columbia	51.5	−122.4	53	0	*Mejia et al.* [2002]
Snake River[b]	43.0	−113.5	26	21	*Tauxe et al.* [2004b]
San Francisco Volcanics[b]	35.3	−111.9	37	0	*Tauxe et al.* [2003]
Azores[c]	37.8	−25.4	35	12	*Johnson et al.* [1998]
La Palma[b,c]	28.8	−17.9	26	8	*Tauxe et al.* [2000]
Mexico	20.1	−99.7	16	7	*Mejia et al.* [2005]
Costa Rica	10.2	−84.4	32	17	Appendix A
Ecuador	−0.4	−78.3	63	13	*Opdyke et al.* [2006]
Atacama	−23.3	−67.7	46	23	Appendix A
Easter Island	−27.1	−109.2	62	0	*Brown* [2002]
Tatara San Pedro, Chile	−36.0	−70.9	193	22	Appendix A
Australia	−37.7	144.2	38	0	*Opdyke and Musgrave* [2004]
Patagonia	−47.0	−71.1	36	34	*Brown et al.* [2004a]
Patagonia	−51.2	−70.6	50	20	*Mejia et al.* [2004]
McMurdo	−78.1	165.4	36	18	*Tauxe et al.* [2004a]
17 studies total			894	226	

[a] Definitions are as follows: Region, geographical area of study; λ, mean study latitude in degrees (positive north); ϕ, mean study longitude in degrees (positive east); N_{total}, total number of sites with declination and inclination measurement pairs; N_{dated}, number of sites for which new radiometric (usually $^{40}Ar/^{39}Ar$) dates were obtained; and Reference, publication in which the paleomagnetic study is reported. Data not yet published are reported in Appendix A.

[b] Data from the San Francisco volcanics, Snake River plain, and La Palma were included in the regional compilations for the SW USA, NW USA, and Canaries, respectively (see Table 1).

[c] Data sets from the Azores and La Palma were collected prior to the TAFI project but lab protocols followed those of TAFI and so the data sets are included.

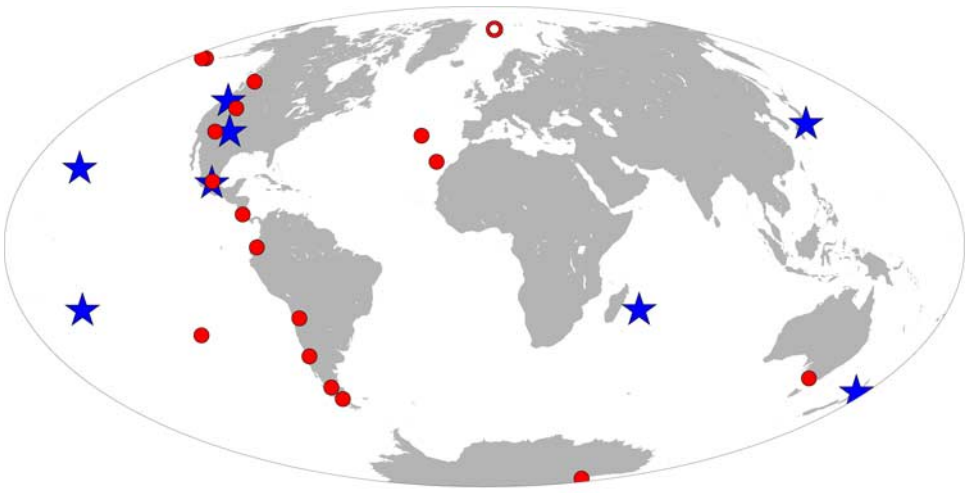

Figure 3. Locations of TAFI sites (red circles, Table 2) and regional compilations from literature (blue stars, *Tauxe et al.* [2003, 2004b], *Lawrence et al.* [2006], and this study, Table 3). Open circle denotes Spitzbergen site, where data are mostly older than 5 Ma and not reported here.

Δ_i represents the angular deviation of the pole for the *i*th site from the geographic north pole, N is the number of sites, and S_B represents the geomagnetic signal remaining after correcting for the within-site dispersion S_{w_i} determined from N_{s_i} samples. (Note that this equation corrects an error in equation (4) of *Lawrence et al.* [2006]). The estimate k for directions can be converted to an approximation to the precision parameter for VGPs using the transformation provided by *Creer* [1962]. The statistical approach inherent in using S_B circumvents the lack of detailed age control and the absence of time series of observations that are inevitable in working with lava flows from disparate locations.

[10] While there have been previous attempts to compile global data sets suitable for TAF and PSV modeling [*McElhinny and Merrill*, 1975; *Lee*, 1983; *Quidelleur et al.*, 1994; *Johnson and Constable*, 1996], many issues have plagued interpretations, notably those of inadequate (or even unknown) temporal sampling, poor geographical coverage, and poor data quality resulting from inferior laboratory methods. These limitations are the cause of much of the discussion surrounding the level of complexity in the 0–5 Ma TAF. The most conservative view is afforded by *McElhinny and McFadden* [1997] (hereafter MM97), who in an assessment of a global paleomagnetic database concluded that only 394 D, I pairs would meet modern standards for paleomagnetic research. These data (designated by a demagnetization code 'DMAG 4' in work by MM97) are restricted to 8 globally distributed locations, and have poor age control (Table 1). This does not necessarily mean that the older data are unusable, but has provided a strong incentive to understand the influence of data quality in their interpretation [e.g., *Tauxe et al.*, 2003; *Lawrence et al.*, 2006].

[11] In this paper we provide a synthesis of ongoing work toward new global data compilations for TAF and PSV modeling. In particular, we report the collective results of a major multi-institutional effort, the Time-Averaged Field Investigations (TAFI) project, to improve the characterization of the time-averaged geomagnetic field and paleosecular variation over the past 5 million years. Results of individual studies from this project have been reported in several publications (see Table 2); here we investigate new constraints these data place on global paleofield behavior. We summarize the numbers of data collected, common field and laboratory procedures, and the resulting temporal and spatial data distribution. We investigate the influence of data quality and transitional sites on estimates of the TAF and PSV from the TAFI data. We supplement the TAFI data with recently published regional compilations, and two new compilations for New Zealand and Japan that we report here. The resulting data set, while not comprehensive, provides a significant improvement over existing global data sets, and we use it to investigate zonal (latitudinal) structure in the TAF and PSV.

2. Time-Averaged Field Investigations (TAFI) Project

[12] Paleomagnetic directions have been obtained from 894 lava flows at 17 locations (Figure 3); we

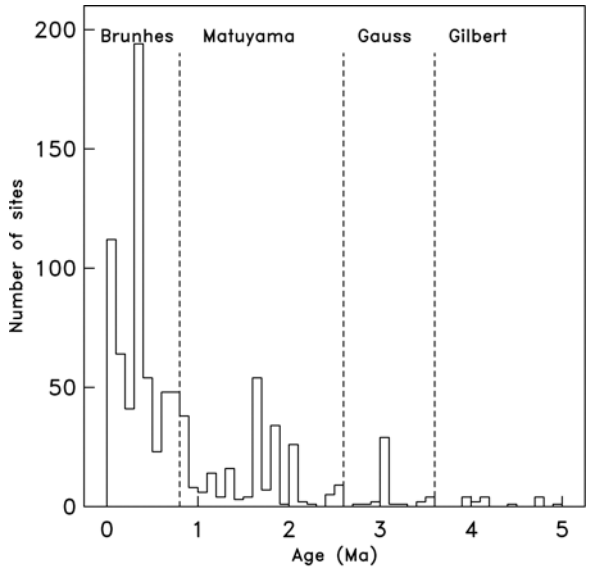

Figure 4. Age distribution for the 883 TAFI sites with ages less than 5 Ma. Average age and an estimate of error in the age are obtained via one of the following: (1) radiometric dates obtained as part of the TAFI project (226 flows), (2) previous radiometric ages made directly on TAFI sites (≈90 flows), or (3) inferred age: stratigraphy and/or polarity chron (remaining flows).

refer to each location as a study. The TAFI study locations were chosen to improve the geographical coverage of 0–5 Ma paleomagnetic directions at high latitudes (Spitzbergen, Aleutians, Antarctica), and in the Southern Hemisphere (various South American locales, Easter Island and Australia). Samples in four studies, Aleutians [*Stone and Layer*, 2006; *Coe et al.*, 2000], Antarctica [*Tauxe et al.*, 2004a], and Easter Island [*Brown*, 2002], were collected in the 1960s and 1970s, but original laboratory measurements involved minimal demagnetization. For these studies modern demagnetization techniques were applied to existing paleomagnetic cores. For the other 13 studies, new field work was required. New radiometric dates, along with 95% uncertainties were obtained for 226 of the TAFI sites (Table 2). Previously obtained radiometric dates are available for 88 additional flows. Ages were assigned to the remaining sites on the basis of absolute and relative age data provided in the original TAFI publications. In some cases only the polarity chron is known, and a median chron age, with uncertainties corresponding to half the chron length were assigned. Thus assignments of age and age uncertainty have been made for all TAFI sites. 883 sites have ages less than 5 Ma, the majority are of Brunhes (67%) or Matuyama (26%) age (Figure 4).

2.1. Paleomagnetic Field Procedures and Laboratory Methods

[13] Sampling was restricted to lava flows or thin dikes: units that cool quickly, and can record the instantaneous geomagnetic field at the time and location of emplacement of the volcanic unit. Standard 2.5-cm-diameter paleomagnetic cores, about 10 cm long, were drilled in the field. Each site was determined to be in situ; postemplacement tilting was avoided. Outcrops were surveyed using a magnetic compass and/or a Bartington magnetometer to minimize sampling of units subjected to lightning strikes. For each study, as many sites were sampled as possible during the field season, with a goal of at least 10 sites for a given polarity. On average, about 50 sites were obtained per study (Table 2). A minimum of 10 cores were drilled over a several-meter-extent of outcrop to allow assessment of orientation error at each site. (The data set from La Palma [*Tauxe et al.*, 2000] preceded these standards and 5–12 samples per site were drilled.) Each sample was oriented using a magnetic compass, and where possible a sun compass and/or back-sighting (see *Tauxe et al.* [2003] for details).

[14] Laboratory methods vary slightly among studies, but a set of minimum criteria were adopted: In all cases natural remanent magnetizations were measured for all specimens, and one specimen per core for at least 5 cores (samples) per site, was subjected to stepwise alternating field or thermal demagnetization. Accompanying rock magnetic measurements, such as susceptibility and Curie temperature were also made. New $^{40}Ar/^{39}Ar$ radiometric ages were obtained for lava flows from twelve studies. Details of the paleomagnetic and age measurements, and resulting data for each study are given in the original publications of paleomagnetic results [*Brown*, 2002; *Brown et al.*, 2004a; *Johnson et al.*, 1998; *Mejia et al.*, 2002, 2004, 2005; *Opdyke and Musgrave*, 2004; *Opdyke et al.*, 2006; *Stone and Layer*, 2006; *Tauxe et al.*, 2000, 2003, 2004a, 2004b]. In this paper we use site mean directions as follows. Original data, including all laboratory and field measurements, from the Azores [*Johnson et al.*, 1998], La Palma [*Tauxe et al.*, 2000], Southern Patagonia [*Mejia et al.*, 2004], Antarctica [*Tauxe et al.*, 2004a], Snake River [*Tauxe et al.*, 2004b], San Francisco Volcanics [*Tauxe et al.*, 2003], and Costa Rica (C. G. Constable et al., manuscript in preparation, 2008, and Appendix A) have been archived in the MagIC database [*Solheid et al.*, 2002] (http://www.earthref.org/MAGIC/).

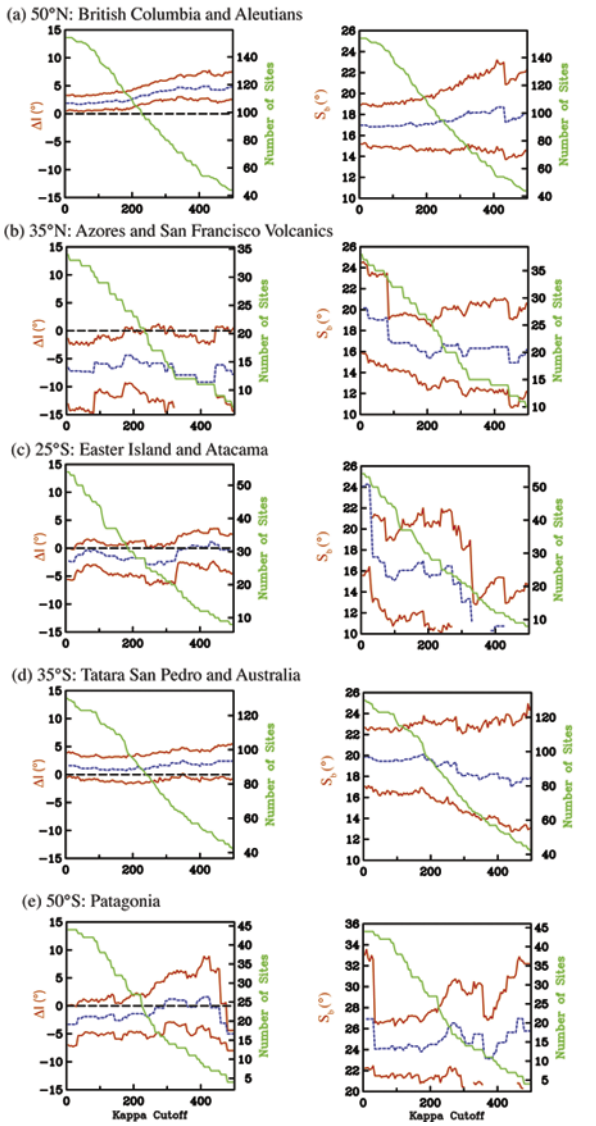

Figure 5. Inclination anomaly (ΔI) and VGP dispersion (S_B) versus cut-off value of k (k_{cut}) for five latitude bins of the TAFI data set. Normal polarity data are shown, and only sites with $n \geq 5$ (at least five samples per site) are considered. Mean ΔI, S_B (blue curves) along with the bootstrap 95% confidence intervals (red curves) are shown. Green curves indicate number of contributing data at each value of k_{cut}.

Sample-level directions reported in MagIC use principal component analysis and require at least 4 demagnetization steps and a maximum angular deviation of the data about the stable component of less than 5°. Fisher mean directions were computed for all sites with at least 3 samples per site. Over 80% of these sites have site mean directions derived from at least 5 samples. For all other studies (Aleutians [*Stone and Layer*, 2006], Nunivak [*Coe et al.*, 2000] (Appendix A), British Columbia [*Mejia et al.*, 2002], Mexico [*Mejia et al.*, 2005], Atacama and Tatara San Pedro, Chile [*Brown et al.*, 2004b] (Appendix A), Easter Island [*Brown*, 2002], Patagonia [*Brown et al.*, 2004a]) we have used the site mean directions reported in the original publication or in Appendix A. In this paper we use only paleodirections, as absolute paleointensity mesurements are still underway for several of the TAFI studies. For all TAFI studies, the site-level results used in this paper are archived in the MagIC database, including the data reported in Appendix A [*Solheid et al.*, 2002] (http://www.earthref.org/MAGIC/).

2.2. Assessment of TAFI Data Quality

[15] As has been discussed extensively [e.g., *McElhinny and McFadden*, 1997; *Johnson and Constable*, 1996; *Merrill et al.*, 1996], assessment of data quality is critical to accurate identification of paleosecular variation and of non-GAD time-averaged field structure. Typically site mean directions with an associated α_{95} greater than (or k less than) a certain value are excluded from analyses. Recent regional data compilations consist of several hundred site mean directions, and enable an assessment of the behavior of TAF and PSV estimates as increasingly stringent data quality requirements are imposed. We use a similar approach to that reported by *Tauxe et al.* [2003] (hereafter T03) and by *Lawrence et al.* [2006] (hereafter L06).

[16] Our measure of data quality for individual sites is k. We use inclination anomaly, ΔI, (equation (3)) to characterize the TAF, and between-site VGP dispersion, S_B, (equation (4)), for PSV. We calculate ΔI and S_B using site mean directions with values of k greater than a cut-off value, denoted by k_{cut}. Increasingly stringent data quality criteria correspond to successively larger values of k_{cut}. The approach is discussed in detail by L06 and we do not repeat it here. The TAFI data set differs from those of T03 and L06, having sites from a broad range of latitudes, and we expect both PSV and TAF estimates to include a latitudinal signature. We investigate the TAFI data set by binning data from similar latitudes, but retain a distinction between northern and southern latitudes. Sufficient data are available at latitudes of approximately 50°N, 35°N, 25°S, 35°S, and 50°S to perform an investigation of how ΔI and S_B vary with k_{cut}. We use only sites for which the number of samples per site, n, is at least 5 because lower n leads to less reliable estimates of k (see, e.g., T03). The results are shown in Figure 5 for normal polarity data

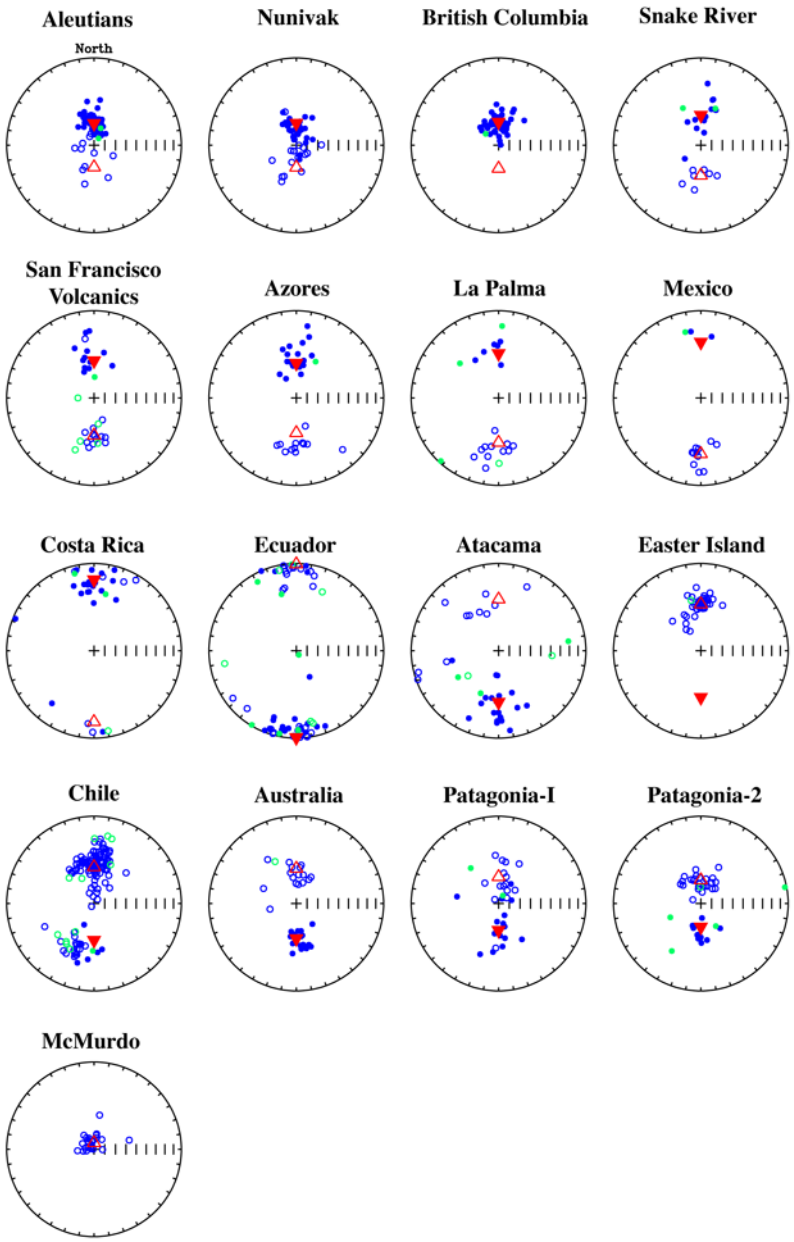

Figure 6. Equal area projections of site directions for each of the 17 TAFI studies,for sites with $n \geq 5$. Solid (open) circles represent projections onto the lower (upper) hemisphere. Sites with estimates of the within-site Fisher precision parameter $k \leq 50$ are shown in green, and those with $k > 50$ are shown in blue. No VGP latitude cut-off is applied; that is, transitional directions, if present, are included. The GAD field direction at the mean site location is given by the red triangle. North is 0° declination.

only, since these dominate our data set. Normal polarity is defined here as site mean directions that have a corresponding positive VGP latitude; thus no distinction between stable polarity and transitional data is made in the evaluation of data quality.

[17] Taken together, these regional analyses indicate that inclination anomaly is quite robust with respect to data quality, especially in regions with large data sets. For example, the latitude band with the most data, centered on 35°S, shows an average inclination anomaly that is small (≈2°) and positive, and does not change significantly as the value of k_{cut} is varied. For other regions, there is some change in the estimate of ΔI at high values of k_{cut} because the smaller data sets yield less reliable results. The behavior of S_B with k_{cut} varies from region to region. Two latitude bands (50°N and

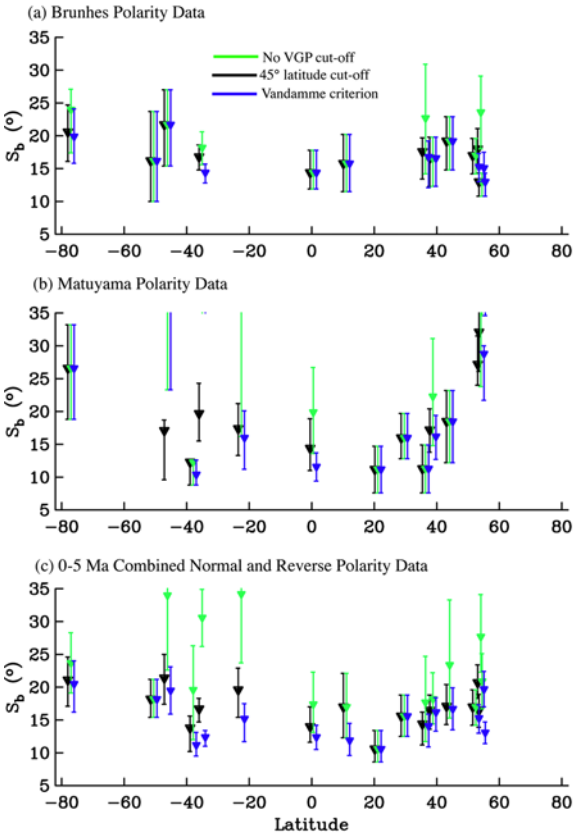

Figure 7. Effect of VGP latitude cut-off on estimates of dispersion for the TAFI studies for (a) Brunhes-age normal polarity data, (b) Matuyama-age reverse polarity data, and (c) 0–5 Ma combined normal and reverse polarity data. A constant 45° cut-off (black), the Vandamme criterion (blue), and no cut-off (green) are shown.

35°S) show no change in the estimate of S_B at low k, two latitude bands (25°S and 50°S) show a decrease in S_B of 2°–6° at values of k_{cut} around 50, and one latitude band (35°N) shows a change in behavior at around k_{cut} = 100. The low-quality data can result in overestimates of VGP dispersion. Our current data set is not able to resolve any latitudinal trend in this bias. For latitudes 50°S, 25°S, 35°N, values of k_{cut} of 250 or more result in noisy estimates of S_B due to the small number of data retained. Analysis of reverse polarity TAFI data showed similar behavior as a function of k_{cut}, although estimates of both S_B and ΔI display more scatter owing to the much smaller data sets.

[18] On the basis of these results we use the following data selection criteria for further analyses of TAFI data: we require (1) $n \geq 5$, (2) $k > 50$. The one exception to this is the data set from Easter Island for which only 4 cores were available for study. In this case we require $n \geq 4$, and $k > 50$ in order to retain geographical sampling. The TAFI data set is summarized in Figure 6 on a study-by-study basis, sites with $k \leq 50$ are distinguished (green) from those with $k > 50$ (blue).

2.3. Effect of Transitional Data

[19] Traditionally, sites with "low" VGP latitudes are removed from studies of PSV and the TAF. This approach has been justified as a means of characterizing stable polarity average field geometry and its paleosecular variation, but it is important to recognize that it may well prejudice our view of the phenomena we want to study. In addition, the choice of which data to exclude is ad hoc. We do not try to resolve this issue here, but show how different criteria for identifying (and excluding) transitional data affect estimates of VGP dispersion determined from the TAFI data set. Given the temporal distribution of the TAFI data (Figure 4), we analyze Brunhes-age normal polarity data, Matuyama-age reverse polarity data, and 0–5 Ma combined normal and reverse polarity data. For each TAFI study we compute S_B using the data quality criteria above, for 3 different choices of VGP latitude cut-off (Figure 7). We compare the use of a constant VGP latitude cut-off (here 45°) with one that is permitted to vary with the empirically derived dispersion as proposed by *Vandamme* [1994]. The Vandamme criterion prescribes a VGP latitude cut-off as

$$\lambda_{cut} = 90^\circ - (1.8S_B + 5)^\circ. \quad (5)$$

S_B is calculated from the data set, then sites with VGP latitudes less than λ_{cut} removed, S_B recomputed, and the procedure repeated; that is, all data are included.

[20] Figure 7a shows that most Brunhes-age TAFI data do not include low-latitude VGPs, and estimates of S_B are in agreement for any choice of VGP cut-off. Field procedures were deliberately focused on obtaining stable polarity data so this is not surprising. For the three Brunhes studies where some low-VGP-latitude data are present, as seen by the higher estimates of S_B for the green (no cut-off applied) versus black or blue (cut-off applied) symbols, the use of the Vandamme or constant VGP cut-off criteria does not significantly alter the estimates of dispersion. For the Matuyama-age data, several studies show high S_B when all VGP latitude data are included. (Note that S_B for the Chilean data at 36°S is greater than 35°, and so plots off the scale of Figure 7, when either no VGP

Table 3. New Zealand Studies[a]

Location	λ, deg	ϕ, deg	$N_{Brunhes}$	$N_{Matuyama}$	Reference
Auckland volcanic province	−36.9	174.8	17	...	*Shibuya et al.* [1992]
South Auckland volcanic province	−37.2	174.9	7	10	*Briggs et al.* [1994]
Taupo ignimbrites[b]	−38.5	176.5	15	...	*Shane et al.* [1994]
Northland	−35.4	174.0	9	2	*Shibuya et al.* [1995]
Central Taupo[c,d]	−38.5	176.0	39	14	*Tanaka et al.* [1996]
Taupo, Ruapehu volcano[d]	−39.3	175.6	27	...	*Tanaka et al.* [1997]
Total			114	26	

[a] Definitions are as follows: λ, mean study latitude in degrees; ϕ, mean study longitude in degrees; $N_{Brunhes}/N_{Matuyama}$, number of Brunhes/Matuyama sites with $n \geq 3$. There are 92 Brunhes sites with $k > 100$ and $n \geq 5$, with a mean direction, $D = 8.2°$, $I = -56.7°$ ($I_{GAD} = 57.5°$) and $\alpha_{95} = 2.1°$. There are 14 Matyuama sites with $k > 100$, $n \geq 5$, with a mean direction, $D = 180.4°$, $I = 62.1°$ ($I_{GAD} = 57.5°$) and $\alpha_{95} = 6.2°$.
[b] Mamaku ignimbrite is excluded since reported directions are anomalous and not well understood.
[c] Directions from Lake Whakamura are excluded since post emplacement tectonics reported.
[d] Directions supercede and replace those of *Cox* [1969, 1971].

cut-off or the Vandamme criterion is applied.) In addition, two of these studies, Patagonia [*Brown et al.*, 2004a] and Chile (Appendix A) [*Brown et al.*, 2004b], show quite different estimates of S_B when the Vandamme versus the constant VGP cut-off criterion is applied. The use of Vandamme's criterion assumes that low latitude VGPs are outliers in the distribution; if several low-VGP-latitude sites are present the Vandamme algorithm will converge without removing these sites. In the case of the Chilean data set, most Matuyama-age sites sample the Matuyama-Brunhes reversal [*Brown et al.*, 2004b], and in the case of the Patagonia data set [*Brown et al.*, 2004a] 5 of the 14 sites meeting our data quality selection criteria have low VGP latitudes. Analyses of the 0–5 Ma data set show several studies for which the Vandamme and constant cut-off criteria give different estimates of S_B. This results from combining normal and reverse polarities that may individually have different estimates of S_B and different VGP latitude populations.

[21] In summary, Figure 7 shows that most TAFI studies contain few or no low-VGP-latitude data. However, in the cases where such data are present the Vandamme and constant VGP cut-off criterion can result in different estimates of S_B, especially when normal and reverse polarity data are combined. Because we wish here to focus on stable polarity field behavior, we choose to remove low-VGP-latitude sites. On the basis of the above analyses, we choose to use the constant VGP cut-off criterion and exclude sites with VGP latitudes less than 45°. Importantly, we note that in comparing the predictions of statistical models with data the same criterion can be applied to simulations from statistical models as to the data, and so our choice is not restrictive. After removal of low-k and low-VGP-latitude sites, our TAFI data contribute 661 sites.

3. Additional Data

[22] We supplement the TAFI data with eight regional data sets based on compilations from the literature; consequently these are more heterogeneous in associated age information, sampling and laboratory procedures than our TAFI data set. Six of the compilations have been described elsewhere: paleomagnetic directions from the NW and SW USA (*Tauxe et al.* [2004b] and *Tauxe et al.* [2003], respectively), Mexico [*Mejia et al.*, 2005; *Lawrence et al.*, 2006], Hawaii, the South Pacific and Reunion [*Lawrence et al.*, 2006]. In three cases, the SW USA, the NW USA, and Mexico, the published regional compilations included data collected as part of the TAFI project (see Tables 1 and 2). In this paper, we analyze all TAFI data together because of their homogeneity in terms of field work and lab protocols. To avoid duplication, the TAFI data from the San Francisco volcanics, Snake River plain, and Mexico are thus removed from the SW USA, NW USA and Mexican regional compilations respectively. We add new data sets for New Zealand and Japan, and summarize these here. Sampling in both Japan and New Zealand has been concentrated on Brunhes or Matuyama age outcrops, and so we investigate these polarity periods only. Paleomagnetic and age data reported in all studies contributing to the regional compilations are available from the MagIC database at EarthRef.org (www.earthref.org/MAGIC).

[23] The volcanic centers of the North Island, New Zealand have been extensively sampled for studies of paleosecular variation, beginning with *Cox*

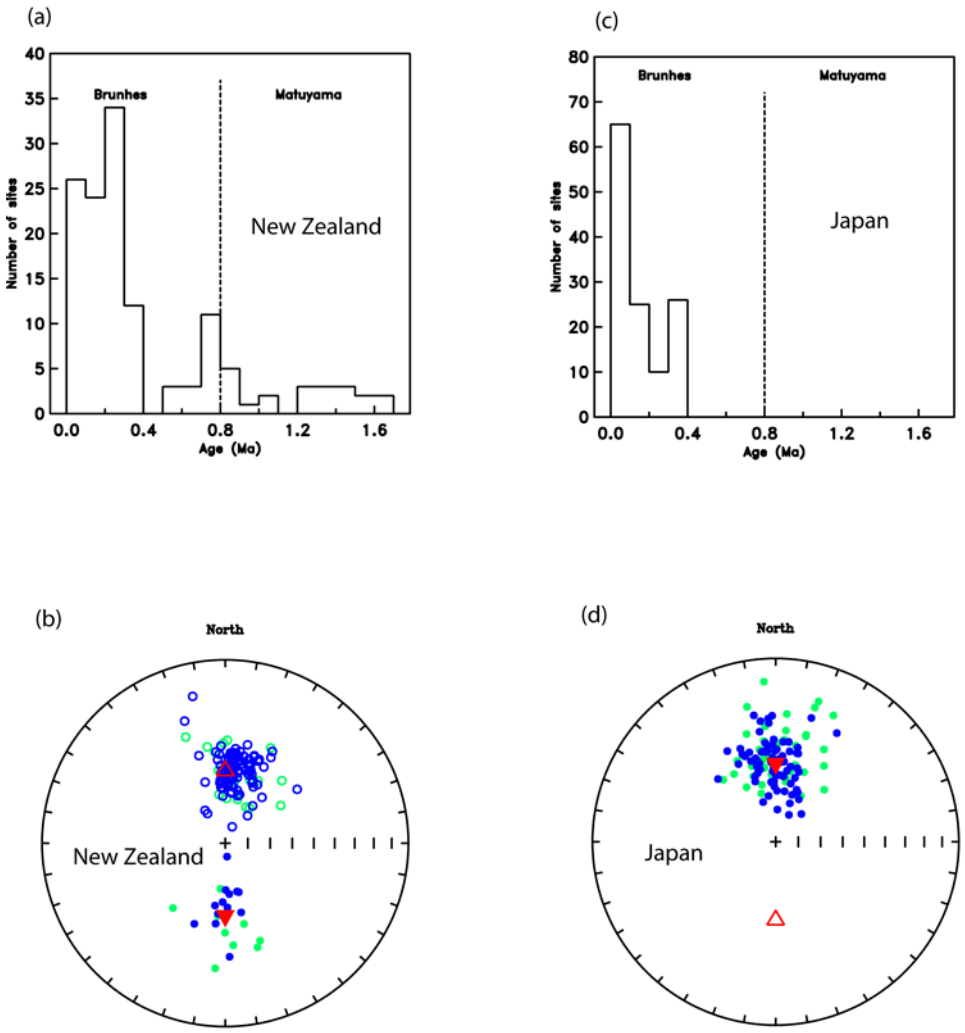

Figure 8. (a, b) New Zealand and (c, d) Japanese data compilations. Age distributions of contributing sites ($n \geq 5$, $k > 100$) are shown in New Zealand (Figure 8a), and Japan (Figure 8c). Equal area projections (figure format as in Figure 6) of site directions are shown in New Zealand (Figure 8b) and Japan (Figure 8d).

[1969, 1971]. Our compilation includes paleodirections from all sites, except those suspected of tectonic rotation and those with fewer than 3 samples. It comprises 140 sites of Brunhes or Matuyama age: flows, dikes, welded tuffs, welded ignimbrites or small domes (Table 3). Of these 140 sites, 112 Brunhes-age sites and 22 Matuyama sites have at least 5 samples and are used here (Figures 8a and 8b). In many studies, radiometric dates were obtained for several of the flows sampled for paleomagnetic purposes. We use directional and age data from sites from the Auckland province [*Shibuya et al.*, 1992], South Auckland province [*Briggs et al.*, 1994], Northland [*Shibuya et al.*, 1995], and the Taupo Volcanic Zone [*Shane et al.*, 1994; *Tanaka et al.*, 1996, 1997]. We take care to avoid samples from the Mamaku ignimbrite, since the origin of anomalous directions from this exposure is debated [*Shane et al.*, 1994].

[24] The data set for Japan comprises 176 sites with at least 3 samples per site, of which 172 are Brunhes age (Table 4). Of these, only 126 Brunhes-age sites have at least 5 samples and are used here (Figures 8c and 8d). As with the New Zealand data set, many of the paleomagnetic studies also report new radiometric dates. The regional tectonics is complicated with block rotations likely affecting some areas including the Izu Peninsula [*Kikawa et al.*, 1989], and we take care not to include such sites. Notably, we do not include here the studies of *Kono* [1968, 1971] that were included in our previous global PSV data compilation [*Johnson and Constable*, 1996]. It is possible that some of these sites are tectonically affected. Furthermore,

Table 4. Japan Studies[a]

Location	λ, deg	ϕ, deg	$N_{Brunhes}$	$N_{Matuyama}$	Reference
Higshi-Izu volcano group	34.0	138.0	22	...	*Heki* [1983]
Kagoshima Prefecture pyroclastics	32.0	131.5	6	...	*Heki* [1983]
Ashitaka dikes	35.2	138.8	35	...	*Tsunakawa and Hamano* [1988]
Ashitaka volcano; Izu-Oshima Isl[b]	35.0	139.0	48	...	*Kikawa et al.* [1989]
Mount Fuji and Mount Oshima	35.4	138.8	6	...	*Tanaka* [1990]
Goto Islands, Tsushima Strait	32.9	128.9	5	...	*Ishikawa and Tagami* [1991]
Zao volcanic group[c]	38.1	140.5	11	4	*Otake et al.* [1993]
Daisen volcano	35.4	133.6	2	...	*Tanaka et al.* [1994]
Shikotsu caldera	42.6	141.3	4	...	*Tanaka et al.* [1994]
Ontake Volcano	35.9	137.5	33	...	*Tanaka and Kobayashi* [2003]
Total			114	26	

[a] Table format is as in Table 3.
[b] We excluded sites from Izu peninsula owing to possible tectonic rotation. There are 80 Brunhes sites with k > 100, with a mean direction, $D = 358.7°$, $I = 54.6°$ ($I_{GAD} = 54.9°$) and $\alpha_{95} = 2.6°$.
[c] We excluded site ZK03, since of Jaramillo age. We also excluded the four reverse polarity sites from our calculations.

other, more recent studies provide paleomagnetic directions at nearby sites, and use modern laboratory methods.

[25] We conducted an assessment of data quality for these new compilations. Estimates of ΔI were found to be robust for all values of k_{cut}. Estimates of PSV are robust for values of k_{cut} up to about 250 (beyond which there are insufficient data to assess PSV), and give $S_B \approx 16°$. Because the data can include studies with minimal demagnetization, we consider sites with $k > 100$ in our further investigations, for compatibility with the other regional compilations used here.

[26] Paleodirections from all contributing sites are shown in Figures 8b and 8d. For New Zealand, 92 Brunhes-age stable polarity sites have $k > 100$ and $n \geq 5$. The distribution of these directions is non-Fisherian (Figure 8b): The mean inclination is compatible with that predicted by GAD, but a significant positive declination anomaly is observed (Table 3). Of the 22 Matuyama sites with $n \geq 5$, 14 have a value of $k > 100$, and the resulting mean direction is compatible with GAD (Table 3). For Japan, 80 Brunhes-age sites have $n \geq 5$ and $k > 100$. The distribution of directions is non-Fisherian, with a mean direction indistinguishable from GAD (Table 4).

4. Toward a New Global Data Compilation: Latitudinal Variations in the TAF and PSV

[27] We combine our TAFI data set with the new compilations from Japan and New Zealand, and previously published compilations for the SW USA [*Tauxe et al.*, 2003], the NW USA [*Tauxe et al.*, 2004b], and 20° latitude [*Lawrence et al.*, 2006]. For the TAFI data we retain sites with at least 5 samples, values of k greater than 50 and VGP latitudes higher than 45°. As noted previously the one exception to this is Easter Island for which we allow 4 samples per site. For the regional compilations we retain sites with at least 5 samples and values of k greater than 100. The higher k cutoff for the regional compilations retains consistency with the original publications of these data sets, and is more conservative because of minimal demagnetization at some sites in older studies. This results in a data set of 2107 (D, I) pairs, compared with 314 (D, I) pairs meeting both these criteria and the DMAG 4 criteria of MM97. The new data set supercedes and replaces all of the MM97 DMAG 4 sites, except those from Iceland, and spans latitudes from 78°S to 53°N. In particular, the TAFI data significantly improve coverage in the Southern Hemisphere. This was previously restricted to 3 locations (Tahiti, Reunion and New Zealand (Table 1), for which the numbers of data have been greatly increased (Table 5)) and now includes TAFI data from 8 additional locations (Table 2). Site level age information is available for all the regional compilations except that from the SW USA [*Tauxe et al.*, 2003]. In that study sites with ages less than 5 Ma were retained, but age information is only reported for those sites dated radiometrically; we use only these sites (Table 5). Examination of the temporal distribution of our data set (Figure 9 and Table 5) shows that sampling is concentrated in the Brunhes, but suggests there are also sufficient data to examine behavior during the Matuyama chron.

Table 5. Numbers of Data Used in This Study[a]

Compilation	N_{used}	N_{Bru}	N_{Mat}	$N_{Gau/Gil}$	Reference
TAFI[b,c]	661	408	194	59	this paper
Japan	80	80	...	...	this paper
New Zealand	106	92	14	...	this paper
Hawaii	727	288	57	382	*Lawrence et al.* [2006]
Mexico	137	44	44	49	*Lawrence et al.* [2006]
South Pacific	209	1	163	45	*Lawrence et al.* [2006]
Reunion	43	31	12	...	*Lawrence et al.* [2006]
N. W. USA	89	62	11	16	*Tauxe et al.* [2004b]
S. W. USA	55	31	12	12	*Tauxe et al.* [2003]
Totals	2107	1037	507	563	

[a] Definitions are as follows: Compilation, data compilation reported by cited reference; N_{used}, all data meeting our selection criteria (sites with at least five samples per site, $k > 100$, and VGP latitude greater than 45°); N_{Bru}, Brunhes; N_{Mat}, Matuyama; $N_{Gau/Gil}$, Gauss and Gilbert age sites combined.
[b] New data from Mexico, the Snake River Plain, and the San Francisco volcanics are included in the TAFI summary numbers and are excluded from the summary numbers for the Mexican, NW USA, and SW USA compilations.
[c] TAFI data set includes the Easter Island data for which four samples per site are allowed (see text).

[28] The new data set although still not global in distribution, overwhelms previous compilations in number, quality and age constraints, and substantially improves geographical coverage and temporal sampling of the Brunhes and Matuyama chrons. Because there are gaps in data coverage (e.g., Europe) we restrict ourselves to investigations of latitudinal structure in the TAF and PSV. We correct for plate motions using the model NUVEL 1-A [*DeMets et al.*, 1994] and our estimates of site age.

4.1. PSV: Latitudinal Variations in VGP Dispersion

[29] We first examine latitudinal variations in dispersion recorded by the individual TAFI studies and regional compilations (Tables 6 and 7 and Figure 10). S_B is calculated using equation (4), and 95% confidence limits estimated using a bootstrap resampling technique. Figure 10 shows less latitudinal variation in dispersion during the Brunhes than the Matuyama, and with the exception of the Hawaiian compilation at 20°N, the data set for the Brunhes suggests a constant dispersion with latitude of around 16°. The Matuyama data set shows several estimates of S_B that are higher than during the Brunhes. This difference in S_B between normal and reverse polarity chrons has been observed many times previously and its origin is still not understood [*McElhinny et al.*, 1996]. The Matuyama data display a stronger dependence on latitude of S_B. It is unclear whether S_B is symmetric about the equator; different behavior is seen in the Northern and Southern Hemispheres, although this could be related to differences in spatial and temporal sampling. We note that the data set from Easter Island, for which we have only 4 samples per site, appears to be compatible with other studies. The study-by-study comparison of S_B indicates regional variations in S_B, for example, at 53°N [*Coe et al.*, 2000; *Mejia et al.*, 2002; *Stone and Layer*, 2006] and at 50°S [*Brown et al.*, 2004a; *Mejia et al.*, 2004]. However, because the numbers of data from individual studies are rather low (7 out of 13 Matuyama TAFI studies have less than 10 contributing sites) detailed comparisons of regional variations in S_B, and assessment of PSV models are not possible.

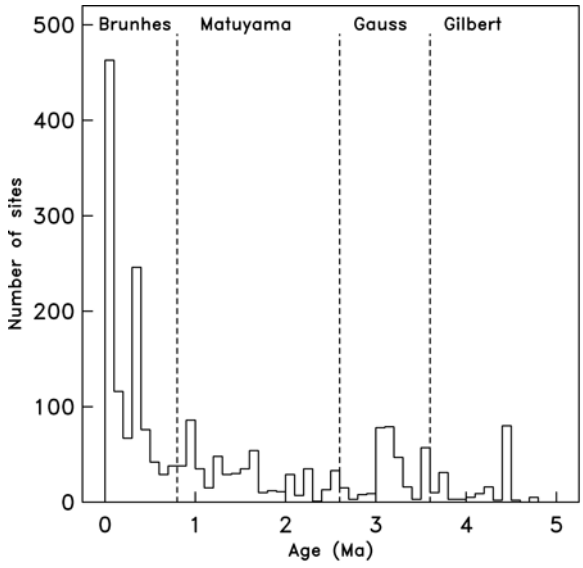

Figure 9. Age distribution for the combined data set of 2107 pairs of declination and inclination measurements (TAFI data plus regional compilations)used in the remaining analyses.

Table 6. TAFI Studies: VGP Dispersion Versus Latitude for the 17 TAFI Studies[a]

$\bar{\lambda}$, deg	N_{Bru}	$S_B{}^{hi}_{lo}$	N_{Mat}	$S_B{}^{hi}_{lo}$	N_{total}	$S_B{}^{hi}_{lo}$
−78.0	27	$20.6^{24.7}_{16.1}$	6	$26.6^{33.2}_{18.8}$	34	$21.1^{24.6}_{17.1}$
−51.5	9	$16.2^{23.7}_{10.0}$	...	...	35	$18.2^{21.2}_{15.4}$
−47.1	11	$21.7^{27.0}_{15.4}$	9	$17.1^{18.7}_{9.6}$	25	$21.4^{25.0}_{17.4}$
−38.9	...	...	21	$12.3^{12.6}_{8.8}$	35	$13.8^{15.6}_{10.2}$
−36.0	102	$16.8^{18.6}_{14.8}$	6	$19.7^{24.3}_{15.5}$	111	$16.7^{18.3}_{14.7}$
−27.0	40	$12.8^{16.8}_{8.4}$	–	–	40	$12.8^{16.8}_{8.4}$
−23.5	...	...	12	$17.4^{21.2}_{13.3}$	27	$19.6^{22.9}_{15.4}$
−0.5	13	$14.4^{17.8}_{11.9}$	26	$14.7^{19.3}_{11.3}$	46	$14.0^{17.0}_{11.6}$
10.0	18	$15.2^{20.2}_{10.6}$	...	...	25	$17.4^{22.5}_{13.4}$
20.2	...	...	9	$11.2^{14.7}_{7.6}$	13	$10.6^{12.5}_{8.6}$
28.6	...	...	11	$16.0^{19.7}_{12.8}$	17	$15.6^{18.8}_{12.5}$
35.4	12	$17.6^{19.7}_{13.4}$	11	$11.3^{14.9}_{7.6}$	24	$14.4^{16.2}_{11.2}$
37.8	19	$16.6^{19.8}_{12.3}$	9	$17.2^{20.4}_{13.8}$	30	$16.5^{18.8}_{13.6}$
43.1	10	$19.2^{22.9}_{14.8}$	6	$18.5^{23.2}_{12.2}$	20	$17.1^{20.4}_{14.3}$
51.5	50	$17.0^{19.6}_{14.2}$	...	...	50	$17.0^{19.6}_{14.2}$
53.1	36	$18.0^{21.1}_{15.3}$	14	$27.2^{31.5}_{24.0}$	50	$20.7^{23.4}_{18.3}$
53.5	47	$13.0^{14.3}_{10.8}$	9	$32.1^{40.1}_{26.1}$	71	$16.5^{18.9}_{13.9}$

[a] Definitions are as follows: N_{Bru}, N_{Mat}, and N_{total}, number of Brunhes-age normal polarity, Matuyama-age reverse polarity, or 0–5 Ma normal and reverse polarity data combined; λ, mean latitude in degrees for the Brunhes, Matuyama, and 0–5 Ma combined data sets; $S_B{}^{hi}_{lo}$, the between-site VGP dispersion in degrees, along with the 95% confidence limits.

[30] To improve temporal sampling, we bin our data set into latitude bands governed by the distribution of sampling sites, and no more than ±5° in spatial extent. S_B is reported for latitude bands with more than 10 sites; the exception is the Matuyama estimate of S_B at Antarctica. This has only 6 contributing sites, but the value of S_B is supported by recent measurements on additional data (K. Lawrence et al., unpublished data, 2008), and this datum provides critical latitudinal coverage. VGP dispersion for the latitudinally binned Brunhes, Matuyama and 0–5 Ma data sets is shown in Figure 11 (values are given in Table 8), and compared with predictions from two paleosecular variation models: Model G [*McFadden et al.*, 1988] and TK03 [*Tauxe and Kent*, 2004]. The TK03 predictions assume a TAF specified by GAD, and 10,000 simulations were made at latitude increments of 5°. Sites with VGP latitudes less than 45° are excluded from the simulated data sets. In addition, for each temporal subset of the data we show the mean S_B calculated from the data. We note that the statistical model of *Constable and Parker* [1988] predicts almost constant S_B with latitude.

[31] The Brunhes age data display little variation in S_B versus latitude in the Northern Hemisphere; the only exception is low secular variation at 20°N that results from the Hawaiian data set [*Lawrence et al.*, 2006]. Overall these data are compatible with a range of models, from those that predict a constant S_B with latitude to those that show some latitudinal variation (such as Model G and TK03).

[32] The Matuyama data show some dependence of S_B on latitude, although, given the restricted data set, it is difficult to discriminate among PSV models. None of the existing models appear satis-

Table 7. Regional Compilations: VGP Dispersion Versus Latitude for the Eight Regional Compilations Given in Table 5[a]

$\bar{\lambda}$, deg	N_{Bru}	$S_B{}^{hi}_{lo}$	N_{Mat}	$S_B{}^{hi}_{lo}$	N_{total}	$S_B{}^{hi}_{lo}$
−38.2	92	$15.3^{17.5}_{13.1}$	13	$16.4^{23.2}_{10.6}$	106	$15.3^{17.6}_{13.3}$
−20.9	31	$12.8^{15.6}_{9.9}$	...	...	43	$14.5^{16.9}_{12.2}$
−17.9	...	...	81	$19.3^{22.0}_{16.4}$	207	$17.8^{19.4}_{16.0}$
19.9	285	$9.9^{10.9}_{9.0}$	23	$13.1^{17.5}_{8.5}$	681	$14.3^{15.1}_{13.5}$
23.6	44	$17.3^{21.0}_{13.6}$	21	$14.6^{18.3}_{10.8}$	123	$15.9^{17.7}_{14.0}$
35.2	80	$15.1^{17.0}_{13.0}$	...	...	80	$15.1^{17.0}_{13.0}$
36.1	30	$15.9^{18.9}_{13.1}$	12	$18.0^{22.9}_{14.2}$	53	$17.2^{19.7}_{15.0}$
45.5	62	$15.1^{16.8}_{13.4}$	...	...	78	$14.6^{16.2}_{13.3}$

[a] TAFI data from the Snake River Plain, San Francisco volcanics, and Mexico are excluded from the regional compilations. Table format is as in Table 5.

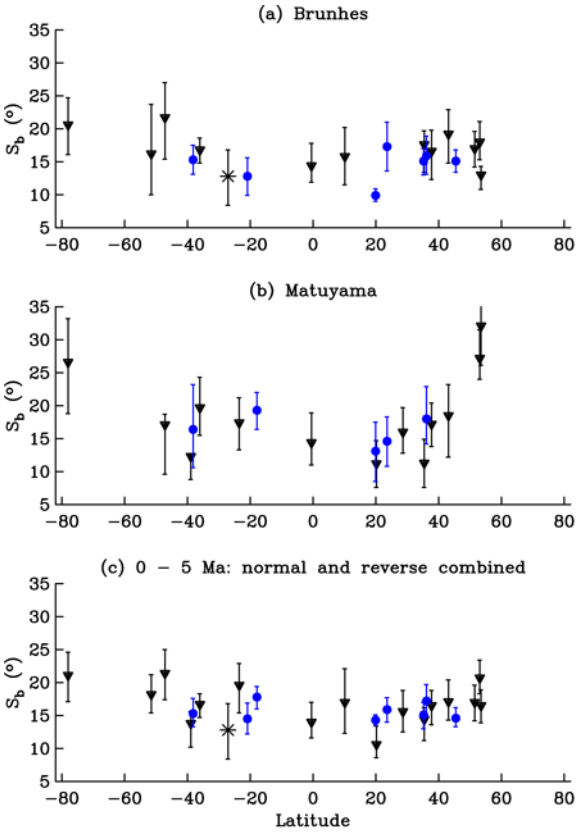

Figure 10. VGP dispersion versus latitude for the TAFI studies (black triangles for all sites with $n \geq 5$ and star for Easter Island, where $n \geq 4$) and regional compilations (blue circles) for (a) Brunhes-age normal polarity data, (b) Matuyama-age reverse polarity data, and (c) 0–5 Ma combined polarity data. (See also Tables 6 and 7 and text for data selection criteria.)

factory; Model G and TK03 fit some data, but data sets at around 20°S and 53°N show rather higher dispersion. The data set from the S. Pacific (approximately 17°S) contains a large number of transitional data, whose effect remains evident even when the lowest VGP latitude data are excluded (our cut-off of 45°). Such oversampling of transitional data should not be the case however for the latitude bins at 22°S and 50°N.

[33] For the combined 0–5 Ma data set, S_B appears to show less latitudinal variation than predicted by either Model G or TK03. Reasonable agreement of the data with Model G, and in particular, TK03, is seen at mid northern (20° to 50°) and mid southern (20° to 40°) latitudes, but S_B estimates for data sets from Ecuador, Costa Rica, and the South Pacific are higher than model predictions. Estimates of S_B at Costa Rica and Ecuador may be influenced by the small sample size; additional data are clearly required to better estimate PSV at low latitudes.

[34] Overall our data appear to show different latitudinal structure for the Brunhes and Matuyama data, and analyses of combined normal and reverse data sets are thus difficult to interpret. These conclusions are evident in both the unbinned TAFI data alone, and the latitudinally binned TAFI and regional data sets. In particular, less latitudinal variation is seen for the Brunhes data set, the temporal interval best sampled by our data, than previously proposed. We next ask whether apparent latitudinal structure in S_B can result from the inclusion of lower quality data, because the large numbers of high-quality data are what distinguish our compilation from those previously published.

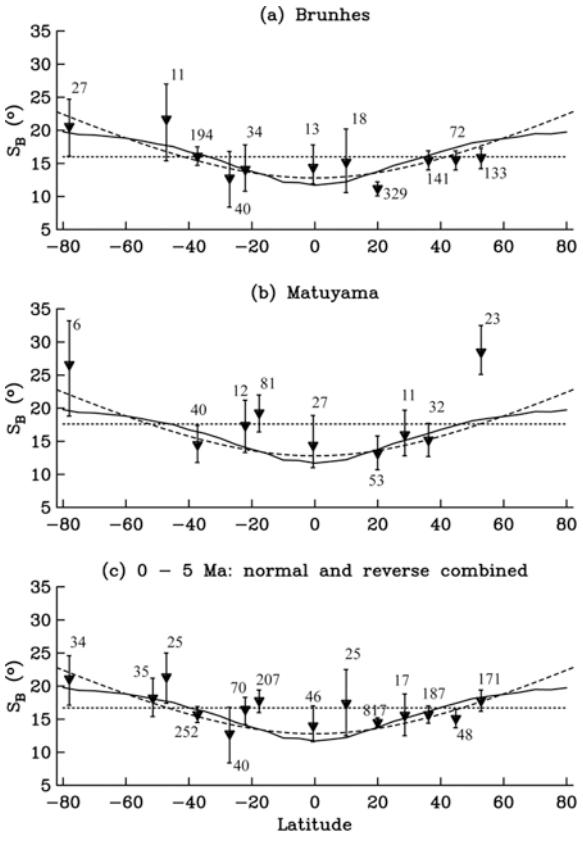

Figure 11. VGP dispersion, S_B (degrees), versus latitude for latitudinally binned data (triangles) with 95% confidence intervals (error bars) for (a) Brunhes-age normal polarity data; (b) Matuyama-age reverse polarity data; and (c) 0–5 Ma data set, normal and reverse data combined. In each plot, the mean value of S_B averaged over all latitude bins is shown (dotted line) as are predicted dispersions for Model G [*McFadden et al.*, 1988] (dashed line) and TK03 [*Tauxe and Kent*, 2004] (solid line). Numbers of data in each bin are indicated.

Table 8. Summary Statistics Versus Latitude[a]

$\bar{\lambda}$, deg	N_{Bru}	$S_B{}_{lo}^{hi}$	ΔI_{lo}^{hi}	N_{Mat}	$S_B{}_{lo}^{hi}$	ΔI_{lo}^{hi}	N_{total}	$S_B{}_{lo}^{hi}$	ΔI_{lo}^{hi}
−78.0	27	$20.6^{24.7}_{16.1}$	$-1.5^{1.6}_{-4.9}$	6	$26.6^{33.2}_{18.8}$	$1.1^{4.1}_{-7.6}$	34	$21.1^{24.6}_{17.1}$	$-1.0^{1.7}_{-4.1}$
−51.4	...	...	...	...	...	...	35	$18.2^{21.2}_{15.4}$	$0.6^{3.0}_{-2.0}$
−47.2	11	$21.7^{27.0}_{15.4}$	$-1.3^{3.6}_{-10.9}$	...	...	...	25	$21.4^{25.0}_{17.4}$	$1.1^{4.8}_{-4.8}$
−37.3	194	$16.1^{17.5}_{14.7}$	$1.8^{3.2}_{0.5}$	40	$14.5^{17.4}_{11.8}$	$1.3^{5.0}_{-2.2}$	252	$15.7^{16.9}_{14.5}$	$1.4^{2.5}_{0.2}$
−27.1	40	$12.8^{16.8}_{8.4}$	$0.0^{1.6}_{-3.1}$	...	...	...	40	$12.8^{16.8}_{8.4}$	$0.0^{1.6}_{-3.1}$
−22.1	34	$14.1^{17.8}_{10.8}$	$-2.4^{1.3}_{-5.5}$	12	$17.4^{21.2}_{13.3}$	$8.2^{15.1}_{-1.9}$	70	$16.5^{18.3}_{14.2}$	$-1.4^{1.7}_{-4.9}$
−17.7	...	...	...	81	$19.3^{22.0}_{16.4}$	$-0.2^{3.7}_{-4.5}$	207	$17.8^{19.4}_{16.0}$	$1.3^{3.9}_{-1.2}$
−0.5	13	$14.4^{17.8}_{11.9}$	$-9.3^{-0.6}_{-17.8}$	27	$14.4^{18.9}_{11.0}$	$-3.2^{0.9}_{-9.1}$	46	$14.0^{17.0}_{11.6}$	$-4.9^{-1.5}_{-9.7}$
10.0	18	$15.2^{20.2}_{10.6}$	$-1.6^{5.1}_{-9.4}$	...	...	...	25	$17.4^{22.5}_{12.5}$	$-3.4^{2.8}_{-10.9}$
20.0	329	$11.2^{12.2}_{10.1}$	$-3.1^{-1.9}_{-4.1}$	53	$13.2^{15.8}_{10.7}$	$-5.3^{-1.8}_{-8.6}$	817	$14.5^{15.2}_{13.8}$	$-5.3^{-4.4}_{-6.1}$
28.6	...	...	...	11	$16.0^{19.7}_{12.8}$	$-7.9^{-5.8}_{-14.7}$	17	$15.6^{18.8}_{12.5}$	$-6.0^{-3.0}_{-11.2}$
36.1	141	$15.5^{16.9}_{14.0}$	$-1.6^{0.1}_{-3.4}$	32	$15.2^{17.7}_{12.7}$	$-6.3^{-2.7}_{-9.6}$	187	$15.7^{17.0}_{14.4}$	$-3.0^{-1.2}_{-4.5}$
44.8	72	$15.6^{16.9}_{14.0}$	$-0.7^{1.6}_{-2.8}$	...	...	...	98	$15.1^{16.5}_{13.7}$	$-1.8^{-0.1}_{-3.5}$
52.8	133	$15.9^{17.3}_{14.2}$	$1.8^{3.3}_{0.9}$	23	$28.5^{32.5}_{25.1}$	$6.0^{11.2}_{1.5}$	171	$17.8^{19.4}_{16.2}$	$2.0^{3.3}_{0.7}$

[a] Definitions are as follows: N_{Bru}, N_{Mat}, and N_{total}, number of Brunhes-age normal polarity, Matuyama-age reverse polarity, or 0–5 Ma normal and reverse polarity data combined; $\bar{\lambda}$, mean latitude in degrees; $S_B{}_{lo}^{hi}$ and ΔI_{lo}^{hi}, the between-site VGP dispersion and the inclination anomaly in degrees, along with their 95% confidence limits.

[35] We compare VGP dispersion as determined from the TAFI data set alone with that calculated for various subsets of the PSVRL database [*McElhinny and McFadden*, 1997]. Figure 12a shows S_B versus latitude for all 0–5 Ma normal polarity data in the PSVRL database with a DMAG code of 2 or greater, and with at least 2 samples per site. There are 2033 data, and these have been binned in 5 degree latitude bins. No further selection for data quality is made. The results show the well-known increase of VGP dispersion with latitude, in both the Northern and Southern Hemispheres. The only data not fit by Model G (TK03 is similar) are those from the S. Pacific (20°S) and about 30 sites from western Canada (58°N). Figure 12b shows the effect of selecting only data with at least 5 samples per site and with k greater than 100. The number of data is drastically reduced (to 714), as seen by the absence in Figure 12b of 3 of the latitude bins present in Figure 12a, and by the increased uncertainties. Notable though is that in several low to mid latitude bins the mean dispersion has increased. In Figure 12c, the data are further restricted on the basis of demagnetization procedure: only data with a *DMAG* code of 3 or greater (i.e., those sites at which all samples were demagnetized) are used. (Restriction to only DMAG 4 results in insufficient data for continued analysis). Only a few latitude bins remain, with a total of 329 data, the dispersion with latitude is approximately flat and is consistent with that measured by the Brunhes TAFI studies. In the experiments shown in Figure 12, the largest effect is contributed by removing sites with inadequate demagnetization suggesting that viscous remanence overprints, if not properly removed can contribute latitudinal structure in S_B.

[36] In a second experiment we use the statistical model of *Constable and Parker* [1988] (hereafter CP88) to investigate how estimates of S_B might be affected by the inclusion of low-quality data with insufficient numbers of samples per site. We choose model CP88 because it predicts flat dispersion with latitude (Figure 13). We simulate 10,000 sites at each latitude, noise is prescribed at the within-site level, by drawing n samples per site, each from a Fisherian distribution with a mean direction given by GAD, and a within-site precision of k. Again, we exclude site mean directions with VGP latitudes less than 45°. Figure 14 shows that with $n = 10$, $k = 100$ the expected flat S_B with latitude is recovered. (Figure 14 also shows model TK03 for reference). Figure 13 shows that as n and/or k are decreased in the simulations, S_B increases (owing to the addition of noisy data), but more importantly apparent latitudinal structure in S_B is introduced. An extreme case in which $n = 2$ and $k = 30$ (for all sites) is shown and indicates that the apparent latitudinal variation in S_B can be quite large (up to 6°). Thus the inclusion of studies with poor quality data or insufficient samples per site could contribute to the observed latitudinal variation in S_B in previous studies.

4.2. TAF: Latitudinal Structure in Inclination Anomalies

[37] We investigate latitudinal structure in the TAF as measured by ΔI. In estimating ΔI, we account for variations in site latitude within a given latitude

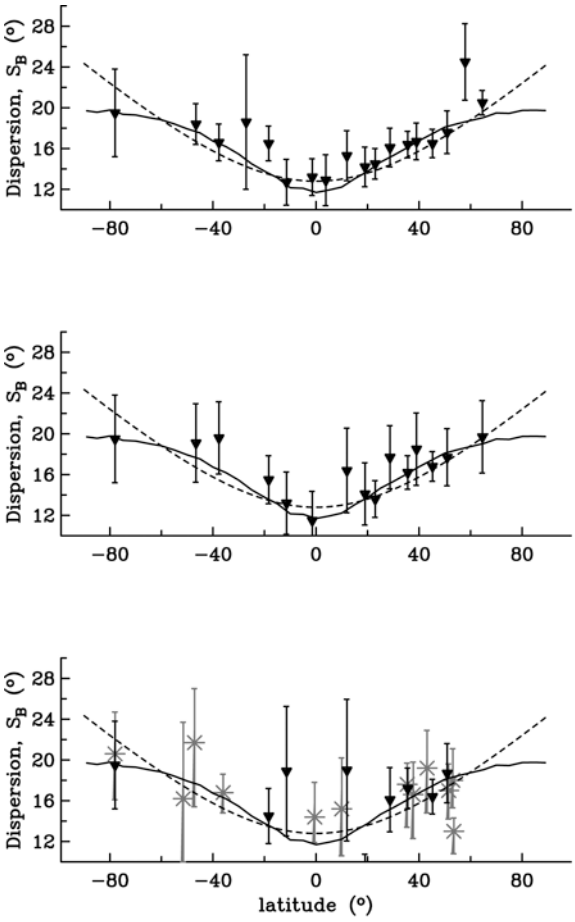

Figure 12. (a) VGP dispersion, S_B (degrees), versus latitude for 0–5 Ma PSVRL normal polarity data binned in 5° latitude bins. Sites with at least 2 samples per site and a *DMAG* code of at least 2 were retained resulting in 2033 data. (b) Further selection of data from Figure 12a, at least five samples per site and $k > 100$ required: 714 datum. (c) Further selection of data from Figure 12b, *DMAG* code of 3 or greater required: 329 data. For comparison, S_B calculated for the Brunhes from the TAFI studies are shown (gray stars and associated error bars). Model G [*McFadden et al.*, 1988] (dashed line) and TK03 [*Tauxe and Kent*, 2004] (solid line) are as in Figure 11.

band as follows. From the observed (D, I) we compute the direction (D', I') relative to the expected GAD direction at the site (i.e., the deviation from GAD). The mean inclination anomaly is computed from the unit vector average of the (D', I') in a given latitude band, and plotted at the mean latitude. The 95% confidence limits on ΔI are calculated using a bootstrap resampling technique. We analyze the Brunhes and Matuyama chrons separately, and the combined normal and reverse polarity data for the 0–5 Ma period. (Normal and reverse data are combined by using the antipode of the reverse polarity directions.)

[38] The results for ΔI are shown in Figure 14 and Table 8. The best geographical coverage is provided by the 0–5 Ma combined data set; however as with S_B, the Brunhes and Matuyama chrons show quite different behavior. Small negative inclination anomalies are seen at most latitudes for the Brunhes; the largest signal is at Ecuador ($\approx -9°$), although the number of contributing data is low (13). Small positive inclination anomalies are seen in the Chilean data set and the binned 50°N data set. The Matuyama inclination anomalies show a quite different structure with pronounced Northern/Southern Hemisphere asymmetry: dominantly negative inclination anomalies in the Northern Hemisphere and zero or positive inclination anomalies in the Southern Hemisphere.

[39] For each temporal subset of the data in Figure 14 we perform a grid search to find the best-fitting two parameter zonal field model to the inclination anomalies. We explore a parameter space in which the g_2^0 and g_3^0 terms can vary from −50% to 50% of the g_1^0 term, in increments of 1%. For each (g_2^0, g_3^0) pair we calculate the weighted root mean square misfit of the predicted inclination anomaly to the observed inclination anomaly. (The weights are determined by the 95% confidence intervals). The best fitting models are provided in Table 9. The Brunhes inclination anomalies are best fit by $g_2^0 = 0.02g_1^0$ and $g_3^0 = 0.01g_1^0$, a result that is similar to previous zonal models for global Brunhes data sets [*Johnson and Constable*, 1995, 1997; *Merrill et al.*, 1996; *Carlut and Courtillot*, 1998]. The larger amplitude Matuyama inclination anomalies are best fit by both larger axial quadrupole and axial octupole terms, with $g_2^0 = 0.04g_1^0$ and $g_3^0 = 0.05\ g_1^0$. Larger amplitude inclination anomalies during reverse polarity periods have long been noted, although their cause (geomagnetic versus rock magnetic [see, e.g., *Merrill et al.*, 1996] has been debated. Large octupole contributions during reverse polarity periods have also been suggested by recent high-quality data sets [*Opdyke et al.*, 2006]. The 0–5 Ma combined normal and reverse polarity data are fit by a two parameter model in which $g_2^0 = 0.03g_1^0$ and $g_3^0 = 0.03g_1^0$. Note that the octupole term here is smaller than that obtained by *Lawrence et al.* [2006] for two reasons. First the data set used here supercedes that of *Lawrence et al.* [2006]; the majority of sites are the same but there are some differences, notably the inclusion of the New Zealand and Japanese data. Second, here we find

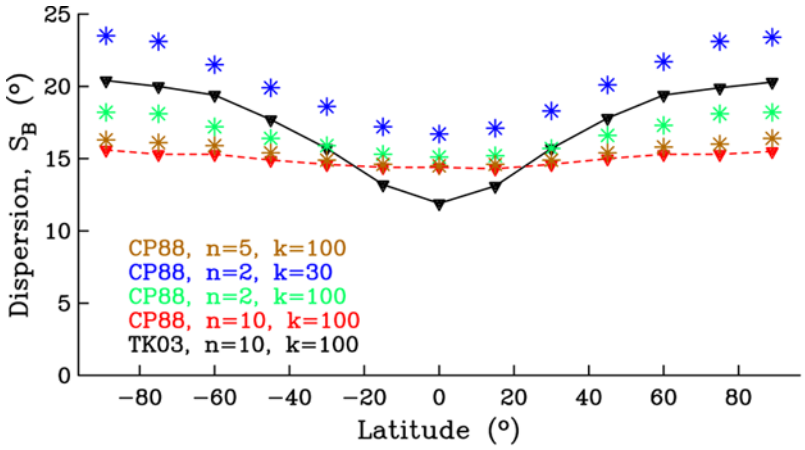

Figure 13. Simulations from statistical model CP88 [*Constable and Parker*, 1988] to show how the numbers of samples per site, n, and data quality as measured by κ can affect the latitudinal variation in VGP dispersion. Model TK03 [*Tauxe and Kent*, 2004] is also shown for reference.

a best fitting two-parameter model to the mean inclination anomaly, weighted by the uncertainties in the mean, whereas *Lawrence et al.* [2006] fit the site level inclination data.

[40] It has long been known [*Creer*, 1983] that biased estimates of direction are obtained when unit vectors are averaged. The bias is manifest as deviations of inclination from GAD predictions that are well approximated by a zonal octupole contribution. We assess the plausible magnitude of such a signal in our data set using a statistical model for PSV [*Constable and Johnson*, 1999]. The TAF structure in the simulations is prescribed as purely g_1^0 (i.e., the time-averaged value of all other spherical harmonic terms is set to zero), and PSV is given by the statistics of the spherical harmonic coefficients prescribed by *Constable and Johnson* [1999]. We simulate directions at our observed site locations, by drawing n samples per site from a Fisherian distribution, with a Fisher precision parameter given by the observed within-site k. The mean inclination is computed for a given latitude band in the same way as for our data. Averaging of unit vectors produces an apparent inclination anomaly versus latitude signature that is best fit (using the grid search algorithm described above) by a $g_2^0 = 0.0$ term, and $g_3^0 = 0.02\ g_1^0$. The same result is obtained if we use the statistical model of *Tauxe and Kent* [2004]. We note that although these simulations (using our site locations and within-site k) suggest a similar bias for the Brunhes, Matuyama and the 0–5 Ma combined data sets, larger bias is incurred if the overall level of PSV is higher [*Johnson and McFadden*, 1997]. Figure 11 suggests higher S_B during the Matuyama,

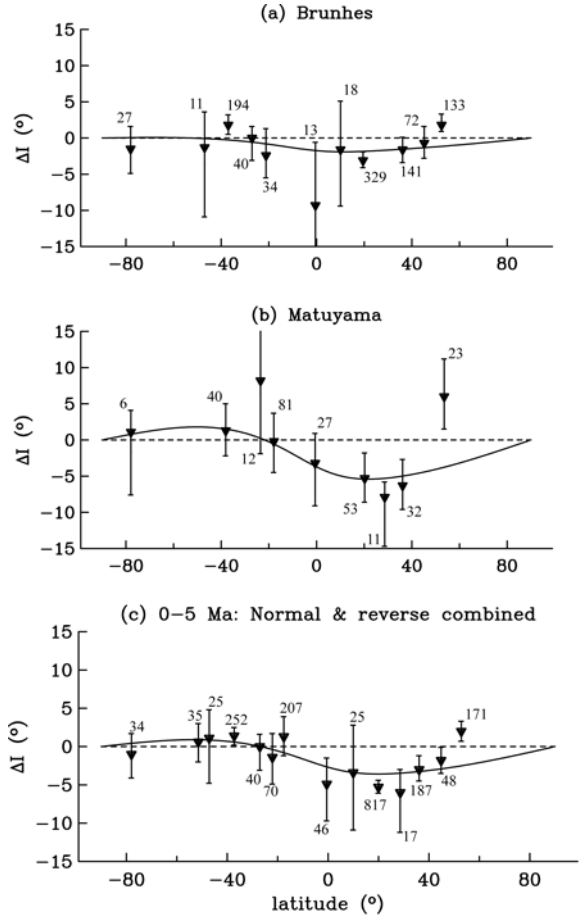

Figure 14. Inclination anomaly versus latitude for latitudinally binned data (triangles) with 95% confidence intervals (error bars), and best-fit two-parameter zonal field model (solid line). (a) 0–5 Ma data set, normal and reverse data combined; (b) Brunhes-age normal polarity data; and (c) Matuyama-age reverse polarity data. Numbers of data in each bin are indicated.

Table 9. Best-Fitting Zonal TAF Models

Time Period	$G_2^0 = g_2^0/g_1^0$	$G_3^0 = g_3^0/g_1^0$
Brunhes	0.02	0.01
Matuyama	0.04	0.05
0–5 Ma combined	0.03	0.03

and this could have an associated larger bias in g_3^0. In addition we have only examined latitudinal contributions to PSV and hence to bias. If the observed inclination anomalies are corrected for this bias, then the g_3^0 contributions for the Brunhes, Matuyama, and 0–5 Ma data sets are reduced in amplitude to $-0.01g_1^0$, $0.03g_1^0$ and $0.01g_1^0$, respectively.

5. Summary and Conclusions

[41] The TAFI project has resulted in a new high-quality set of paleodirections from lava flows, suitable for studying the TAF and PSV. Data from 17 locations provide significantly enhanced spatial coverage over previous data sets [*Quidelleur et al.*, 1994; *Johnson and Constable*, 1996] and over the highest-quality data ('DMAG 4') present in the compilation of MM97. The TAFI data set comprises 884 paleodirections in the 0–5 Ma time interval, with most data of Brunhes and Matuyama age (Figure 4 and Table 5). In addition, data collection efforts by other groups have enabled the compilation of eight regional data sets [*Tauxe et al.*, 2003, 2004b; *Lawrence et al.*, 2006] (also this study), which supercede and replace all but one of the locations of DMAG 4 data (Tables 1 and 5). The resulting combined data set allows investigation of PSV and the TAF as a function of latitude during the Brunhes and Matuyama chrons, and for the combined normal and reverse data for 0–5 Ma.

[42] Our new data set confirms that PSV and the TAF have been different during normal and reverse polarity chrons over the past 5 Ma (see review by *Johnson and McFadden* [1997], and specifically during the Brunhes and Matuyama. It has frequently been suggested that such differences can be attributed to greater contamination of reverse polarity data by viscous overprints; this is not the case in our study because all of the TAFI data reported here has been subjected to thorough laboratory cleaning. Non-GAD contributions to the time-averaged field during the Brunhes are smaller relative to g_1^0 than during the Matuyama, consistent with evidence for a stronger virtual axial dipole moment during this time [*Tauxe and Yamazaki*, 2007; *Valet et al.*, 2005]. In addition, the structure of the non-GAD field is different for the Brunhes and Matuyama chrons with a significant axial octupole contribution during the Matuyama.

[43] Best-fit two-parameter zonal models for the time-averaged field structure indicate axial quadrupole contributions to the TAF of 2–4% of the axial dipole term (Figure 9 and Table 7), compatible with previous studies [*Johnson and Constable*, 1995, 1997; *Carlut and Courtillot*, 1998; *Merrill et al.*, 1996]. A substantial axial octupole contribution (≈5% of the axial dipole) is found for the Matuyama chron, with a smaller contribution during the Brunhes (≈1% of the axial dipole). Simulations using statistical models for PSV [*Constable and Johnson*, 1999; *Tauxe and Kent*, 2004] suggest a g_3^0 signature on the order of 2% is attributable to the bias incurred by the averaging of unit vectors.

[44] Evaluations of VGP dispersion from our new data set show only modest agreement with existing PSV models (Figure 11). The Brunhes data indicate little variation of S_B with latitude, the exception being low PSV at Hawaii. The mean value of S_B is 16°. It is difficult to discriminate among a range of PSV models, from those that predict flat dispersion with latitude (such as CP88) to those that predict a latitudinal increase in S_B (Model G and TK03). Improved evaluation of existing models would be possible with larger low-latitude data sets and new data from high northern latitudes.

[45] Tests with the PSVRL database [*McElhinny and McFadden*, 1997], suggest that differences between previous published results for S_B as a function of latitude and our results here are due to the inclusion in earlier studies of low-quality, uncleaned sites with less than 5 samples per site. In addition simulations with statistical model CP88 demonstrate that an apparent latitudinal increase in S_B can be imparted by sites with insufficient samples per site and/or large within-site scatter.

[46] S_B for the Matuyama chron suggests reasonable agreement with models predicting an increase in S_B with latitude; the Antarctica data set clearly currently has insufficient data to assess PSV, but the result is retained here owing to confirmation from more recent work incorporating additional sites (K. Lawrence, unpublished data, 2008). High S_B at 17°S is due to sampling of transitions in French Polynesia, and the use of a VGP cut-off criterion does not completely remove this oversampling effect.

[47] Latitudinal structure in both PSV and the TAF for the 0–5 Ma data sets is compatible with

previous studies (see review by *Johnson and McFadden* [1997]); however, this data set is dominated by Brunhes and Matuyama age sites. Clearly temporal averaging of the data over 5 Ma affords increased numbers of data, and better spatial coverage, but the results are difficult to interpret given the different TAF and PSV structure during the Brunhes and Matuyama chrons.

[48] The new data set is not complete globally. Existing data from Europe, Iceland, and other recent studies still need to be incorporated and it is clear from the results presented here that additional data are needed from several places (notably equatorial and low latitudes, and high northern latitudes) to allow even latitudinal trends in the TAF and PSV to be properly characterized. In this paper we have only considered zonal structure in the field, although it is evident from the 20° latitude compilation of *Lawrence et al.* [2006] and from estimates of ΔI and S_B from the TAFI studies that there are regional differences in the TAF and PSV from data sets at similar latitudes. Rather than excluding lower quality and/or excursional data, future studies can use more sophisticated weighting schemes to allow the incorporation of all observations. In regions where large data sets are available, progress can be made through inversions of regional data sets for TAF and PSV statistics.

[49] Increasing numbers of high-quality absolute intensity measurements, along with time series of relative paleointensity and inclination from sediments means that in the near future it should be possible to combine these disparate data types into more comprehensive models for field behavior. Such studies will require careful internal assessment of each contributing data type. Assessment of one such data type, paleodirections from volcanics, has been reported here, and shows that the combined data collection efforts of the paleomagnetic community over the past decade have resulted in dramatic improvements in spatial and temporal coverage of 0–5 Ma geomagnetic field behavior.

Appendix A: Unpublished Paleomagnetic Data Used in Our Compilation

[50] Paleomagnetic directions on flows from Atacama in Northern Chile, Costa Rica, and Nunivak (Table 2) have not yet been published elsewhere. We provide a very brief description of results at each location and tabulate the directions used in our study.

A1. Atacama, Northern Chile

[51] The Central Volcanic Zone of the Andes Mountains is composed of subduction-related ignimbrites and lava flows of andesitic composition erupted during late Tertiary and Quaternary time. East of the Atacama desert in northern Chile, 23°S latitude, lavas and ash flows range in age from 8 Ma to Holocene. Included in the sampling were Recent flows from the currently active Lascar Volcano and samples from the famous El Laco magnetite body. Progressive alternating-field demagnetization, and principal component analyses yielded directions from 46 sites, with 26 reversed, 10 normal, and 10 sites with transitional or excursional directions, some with poorly defined directions. All are listed in Table A1. The observed dispersion of the poles is considerably larger than that predicted by Model G [*McFadden et al.*, 1988].

A2. Costa Rica

[52] Paleomagnetic samples from Costa Rica were collected in December 1998 and February 2000. At least 10 samples per site were drilled in 33 lava flows/ignimbrites from the Cordilleras Central and Guanacaste, the underlying Canas, Liberia and Bagaces formations and Volcano Arenal. Sample orientation was with sun or magnetic compass. One flow was inadvertently sampled twice and the samples were merged to form the composite site cr422_cr423. Data from different parts of cr035 were inconsistent, and the flow was resampled in a different location as cr405. AF and thermal demagnetization, followed by principal component analysis were used to obtain results from the 32 sites listed in Table A2. Flow ages range from less than 1 ka to about 3 Ma, and there are 27 normal and 5 reverse polarity results.

A3. Nunivak

[53] The Nunivak data set used here resulted from a restudy of a 1964 collection by A. Cox of 59 oriented cores from Pleistocene lava flows on Nunivak Island in the Bering Sea. The 54 originally published paleomagnetic directional results were primarily based on NRMs. A modern study on remaining samples using progressive demagnetization and principal component analysis has essentially confirmed the original results. The new data are given in Table A3.

Table A1. Atacama Paleomagnetic Sites[a]

Site Name	λ_s	ϕ_s	N_{samp}	Dec	Inc	k	λ_V	ϕ_V
AT-1	−23.51	292.31	5	95.2	−38.5	29	4.0	44.2
AT-2	−23.65	292.46	8	182.6	41.6	213	−87.6	209.9
AT-3	−23.63	292.45	4	161.7	35.3	60	−72.5	32.6
AT-4	−23.60	292.44	6	258.1	−39.1	73	−1.4	177.5
AT-5	−23.61	292.43	8	198.2	36.7	427	−72.8	195.3
AT-6	−23.53	292.38	4	193.3	−19.2	16	−54.1	135.1
AT-7	−23.53	292.38	4	349.6	−39.6	112	80.4	206.6
AT-8	−23.49	292.27	7	179.3	47.3	257	−85.0	299.3
AT-9	−23.50	292.25	7	258.2	44.8	133	−20.2	223.2
AT-10	−23.50	292.25	6	250.4	−2.2	76	−17.5	193.1
AT-11	−23.45	292.22	7	312.1	−18.6	72	42.3	210.8
AT-12	−23.34	292.19	7	230.7	−52.7	19	−15.6	154.4
AT-13	−23.35	292.19	3	299.2	−36.7	143	33.9	192.5
AT-15	−23.85	292.50	5	162.3	48.3	575	−73.3	359.7
AT-16	−23.85	292.50	6	182.5	66.9	517	−64.2	288.8
AT-17	−23.85	292.50	3	351.1	−50.0	986	79.5	159.3
AT-18	−23.86	292.51	6	180.0	30.0	142	−82.2	112.5
AT-19	−23.91	292.44	9	181.2	20.6	1338	−76.7	117.6
AT-20	−23.91	292.44	7	171.8	8.8	1095	−69.0	89.1
AT-21	−23.90	292.45	7	82.2	20.5	33	2.7	9.6
AT-22	−23.91	292.45	5	236.9	44.0	9	−38.7	217.2
AT-23	−23.93	292.34	5	255.0	−5.7	414	−12.5	193.5
AT-24	−23.93	292.34	6	161.7	32.0	171	−71.7	39.9
AT-25	−22.85	292.25	4	195.7	23.6	110	−71.7	169.7
AT-26	−22.72	292.20	7	178.1	23.5	472	−79.4	102.1
AT-27	−22.60	292.44	8	320.7	−46.5	295	54.2	185.8
AT-28	−22.66	292.44	10	178.6	21.7	361	−78.5	105.5
AT-29	−22.87	291.73	4	31.9	−49.1	28	60.7	42.6
AT-30	−22.87	291.73	7	333.8	−49.2	56	65.5	179.0
AT-31	−22.88	291.97	8	342.4	−53.5	175	71.0	162.2
AT-32	−23.32	292.17	9	178.4	25.0	261	−79.7	103.4
AT-33	−23.28	292.01	10	185.8	67.2	514	−63.0	283.8
AT-34	−23.21	292.83	8	202.9	46.2	32	−68.9	219.5
AT-35	−23.12	292.50	8	188.3	44.5	156	−81.9	226.2
AT-36	−22.96	292.33	3	202.0	13.7	102	−63.5	168.7
AT-37	−22.92	292.29	6	184.3	29.6	176	−81.9	142.9
AT-38	−22.92	292.23	6	195.4	43.5	102	−75.7	215.3
AT-39	−23.33	292.22	5	347.3	−33.7	238	77.2	222.2
AT-40	−23.32	292.22	4	192.5	33.3	25	−77.2	180.8
AT-42	−22.40	291.97	5	152.7	30.1	100	−63.5	30.7
AT-43	−22.45	292.00	9	317.8	−44.9	185	51.5	187.2
AT-44	−22.59	291.99	7	177.5	20.8	192	−77.9	100.2
AT-49	−23.91	292.32	7	355.4	−46.6	53	84.3	157.6
AT-50	−23.49	292.01	8	181.3	18.6	300	−76.0	117.3
AT-52	−22.69	292.01	6	23.9	−21.1	91	64.3	358.7
AT-53	−22.73	291.96	5	203.8	16.7	308	−63.1	173.9

[a] Definitions are as follows: λ_s, site latitude; ϕ_s, site longitude; N_{samp}, number of samples at the site; k, estimated Fisherian precision parameter; λ_V, VGP latitude; ϕ_V, VGP longitude.

Table A2. Costa Rica Paleomagnetic Sites[a]

Site Name	λ_s	ϕ_s	N_{samp}	Dec	Inc	k	λ_V	ϕ_V
cr017	10.4967	−85.2290	6	15.1	18.1	685	75.1	8.1
cr035	9.9707	−84.1800	10	345.9	9.8	9	75.1	167.0
cr036	9.9707	−84.1798	6	354.6	25.0	133	83.8	217.1
cr037	9.9707	−84.1800	8	359.1	26.8	360	85.7	264.1
cr401	10.0592	−84.0393	7	346.3	−7.3	704	70.6	141.5
cr402	10.0547	−84.0387	4	0.9	−27.6	199	65.3	93.9
cr404	9.8905	−83.8552	8	347.8	5.9	337	76.0	157.2
cr405	9.9718	−84.1801	9	355.6	22.4	562	85.4	207.4
cr406	10.0703	−83.9848	6	0.9	23.1	1797	87.8	300.1
cr407	10.1103	−83.9745	9	218.7	24.0	457	−45.4	215.7
cr408	9.7570	−84.1999	6	14.2	5.1	136	74.2	31.9
cr409	9.9162	−84.4594	8	342.6	23.3	144	72.8	194.6
cr410	9.7480	−84.4435	10	351.5	24.1	142	81.2	205.3
cr411	9.8847	−83.8944	6	23.3	−15.1	788	60.9	42.4
cr412	9.8847	−83.8944	9	30.6	−6.6	113	56.8	28.0
cr414	9.8156	−83.8633	7	6.7	−15.6	81	71.0	75.3
cr415	9.9692	−84.0849	6	358.4	8.1	259	83.9	111.1
cr416	9.9828	−84.3464	8	170.0	−7.7	15	−78.3	334.7
cr417	10.2889	−84.8336	6	23.4	36.6	103	65.3	338.3
cr418	10.4738	−85.0726	8	180.9	−7.5	1302	−83.2	267.3
cr419	10.4710	−85.0748	5	354.0	32.7	233	80.6	237.2
cr420	10.7293	−85.1796	8	7.1	31.3	681	80.7	322.1
cr421	10.4578	−84.6432	4	343.3	30.8	477	72.7	207.9
cr422_cr423	10.4618	−84.6840	12	347.5	33.2	300	75.7	219.2
cr424	10.4587	−84.6793	6	5.7	11.9	1114	82.8	43.1
cr425	10.7838	−85.4258	5	184.7	−17.5	314	−85.0	205.7
cr426	10.4744	−85.0460	8	173.8	7.5	296	−74.5	298.7
cr427	9.9724	−83.7844	7	359.6	44.5	525	73.8	274.9
cr428	10.2594	−84.1769	7	292.2	3.2	86	22.1	183.4
cr429	10.2080	−84.1635	5	355.3	32.6	1190	81.2	245.2
cr430	10.1909	−84.2334	7	356.7	24.9	878	85.7	227.7
cr431	10.0601	−84.0800	6	11.6	34.2	2	75.8	326.8

[a] Definitions are as follows: λ_s, site latitude; ϕ_s, site longitude; N_{samp}, number of samples at the site; k estimated Fisherian precision parameter; λ_V, VGP latitude; ϕ_V, VGP longitude.

Table A3. Nunivak Paleomagnetic Sites[a]

Site Name	λ_s	ϕ_s	N_{samp}	Dec	Inc	k	λ_V	ϕ_V
A21	53	−172	7	30.1	60.2	720	66.6	296.3
A29	53	−172	7	204.3	−57.5	831	−67.6	129.8
A30	53	−172	7	201.9	−53.0	651	−65.1	140.5
A31	53	−172	7	201.3	−58.7	758	−70.1	132.4
A32	53	−172	8	54.8	78.2	534	60.5	227.8
A33	53	−172	8	11.8	72.9	655	81.5	234.2
A34	53	−172	8	10.4	75.4	441	79.0	214.0
A36	53	−172	7	354.0	75.7	716	79.5	172.9
A37	53	−172	8	9.0	75.1	178	79.8	212.6
A38	53	−172	7	357.8	75.3	312	80.6	181.7
A40	53	−172	7	7.7	72.7	880	83.3	225.5
A41	53	−172	7	13.7	73.9	639	79.7	229.6
A42	53	−172	10	17.5	75.0	590	77.2	227.8
A43	53	−172	6	9.5	72.2	748	83.1	235.8
A46	53	−172	7	125.4	−77.3	447	−60.6	325.0
A47	53	−172	8	136.3	−78.0	225	−64.9	328.5
A48	53	−172	8	194.8	−73.6	629	−79.5	53.6
A49	53	−172	7	341.4	−56.9	77	−1.9	22.7
A50	53	−172	8	339.5	81.7	1251	67.6	173.1
A51	53	−172	7	74.4	80.8	92	54.1	218.4
A52	53	−172	8	204.6	−84.1	597	−63.2	18.8
A54	53	−172	8	200.4	−84.3	1264	−63.3	16.7
A55	53	−172	8	344.2	81.4	854	68.8	175.4
A57	53	−172	7	238.0	−63.3	445	−52.1	86.3
A59	53	−172	7	337.1	84.4	169	62.9	178.5
A60	53	−172	7	345.6	84.5	704	63.4	182.0
A62	53	−172	8	224.3	−83.0	641	−61.4	28.4
A63	53	−172	8	108.3	−83.2	642	−55.2	345.3
A64	53	−172	6	90.9	−87.5	270	−52.8	359.7
A65	53	−172	8	171.5	−78.6	489	−74.4	356.1
A67	53	−172	8	338.0	56.6	259	68.0	60.8
A69	53	−172	6	8.5	67.6	263	84.2	300.0
A70	53	−172	8	156.8	80.4	1317	35.4	196.9
A71	53	−172	7	338.1	68.6	87	76.7	102.1
A72	53	−172	8	342.7	69.0	363	79.5	102.1
A73	53	−172	8	336.3	67.7	297	75.2	98.3
A74	53	−172	7	335.6	70.0	228	75.5	111.5
A75	53	−172	8	326.9	66.7	614	69.1	101.1
A76	53	−172	8	334.8	66.4	630	73.7	93.5
A77	53	−172	8	340.3	75.9	455	75.5	150.9
A78	53	−172	7	338.5	75.2	297	75.4	145.2
A79	53	−172	7	11.1	77.1	1548	76.4	208.0
A80	53	−172	7	5.6	78.9	528	74.2	195.5
A81	53	−172	7	3.7	79.6	351	73.1	192.4
A82	53	−172	7	9.2	79.5	1081	72.8	198.8
A83	53	−172	4	3.8	80.0	896	72.3	192.2
A86	53	−172	7	345.7	64.2	117	78.4	66.5
A89	53	−172	8	163.5	80.2	518	34.5	194.5
A90	53	−172	8	167.1	76.5	432	27.8	194.3
A91	53	−172	9	17.1	62.1	266	75.1	311.6
A92	53	−172	7	27.3	72.4	236	73.9	250.5
A96	53	−172	8	70.6	73.8	378	52.3	238.8
A107	53	−172	8	335.6	74.4	380	74.7	138.3
A109	53	−172	7	169.0	−64.8	886	−80.6	240.9
A110	53	−172	6	89.0	−66.5	195	−36.6	313.2
A115	53	−172	5	4.7	69.1	2227	87.1	283.5

[a] Definitions are as follows: λ_s, site latitude; ϕ_s, site longitude; N_{samp}, number of samples at the site; k, estimated Fisherian precision parameter; λ_V, VGP latitude; ϕ_V, VGP longitude.

Table A4. Tatara San Pedro, Chile, Paleomagnetic Sites[a]

Site Name	λ_s	ϕ_s	N_{samp}	Dec	Inc	k	λ_V	ϕ_V
EMU23	−36	289	5	17.4	−46.2	911	73.0	354.2
EMU22	−36	289	5	17.4	−50.6	624	74.8	6.2
EMU21	−36	289	5	17.0	−48.1	488	74.1	358.3
EMU20	−36	289	5	7.4	−42.5	396	77.0	320.4
EMU19	−36	289	3	8.8	−46.8	728	79.1	334.7
EMU18	−36	289	5	12.1	−45.0	639	76.0	340.0
EMU17	−36	289	4	14.0	−45.8	877	75.2	346.6
EMU16	−36	289	5	10.5	−50.3	295	80.0	352.7
EMU15	−36	289	4	17.7	−49.8	833	74.3	4.2
EMU14	−36	289	5	16.6	−51.4	849	75.7	7.9
EMU13	−36	289	5	16.3	−52.6	502	76.3	12.0
EMU12	−36	289	5	11.6	−49.5	892	78.8	352.2
EMU11	−36	289	5	20.4	−46.9	396	71.0	0.3
EMU10	−36	289	5	16.5	−49.9	1055	75.3	2.8
EMU9	−36	289	5	20.9	−56.4	600	73.2	28.6
EMU8	−36	289	5	11.8	−41.7	550	74.3	332.7
EMU7	−36	289	5	16.9	−47.2	606	73.8	355.8
EMU6	−36	289	4	359.9	−69.5	410	72.8	109.3
EMU5	−36	289	3	4.8	−35.3	858	73.0	304.7
EMU1	−36	289	5	6.8	−43.8	406	78.1	320.3
EPW-6-13	−36	289	5	336.2	−79.4	401	54.1	123.1
EPW-6-12	−36	289	4	34.9	−74.7	978	56.5	79.3
EPW-6-11	−36	289	4	26.8	−82.5	402	48.8	99.1
EPW-6-10	−36	289	4	37.6	−79.9	807	50.2	90.4
EPW-6-9	−36	289	5	45.0	−69.5	293	54.4	62.4
EPW-6-8	−36	289	5	350.2	−75.3	1000	63.0	119.1
EPW-6-7	−36	289	6	219.6	−86.5	279	30.5	114.3
EPW-6-5	−36	289	5	14.5	−76.0	312	61.1	95.7
EPW-6-4	−36	289	5	40.4	−84.9	214	43.4	100.1
EPW-6-3	−36	289	5	14.8	−79.5	342	55.4	100.1
EPW-6-2	−36	289	5	353.8	−83.4	252	48.9	111.2
EPW-6-1	−36	289	4	31.1	−80.4	625	51.1	93.8
ESPE-I-38	−36	289	5	11.8	−51.1	499	79.3	359.2
ESPE-I-33	−36	289	4	16.4	−37.1	175	69.0	336.7
ESPE-I-32	−36	289	6	11.5	−39.3	293	73.0	328.3
ESPE-I-31	−36	289	6	16.7	−38.9	589	69.8	339.7
ESPE-I-30	−36	289	6	12.2	−36.5	320	71.0	326.6
ESPE-I-29	−36	289	6	14.2	−40.2	194	72.0	336.2
ESPE-I-28	−36	289	5	16.5	−37.0	361	68.9	336.8
ESPE-I-27	−36	289	6	1.4	−73.0	180	67.4	107.2
ESPE-I-23	−36	289	5	8.4	−31.7	531	69.7	312.9
ESPE-I-22	−36	289	4	14.2	−36.9	359	70.2	331.8
ESPE-I-21	−36	289	4	2.1	−30.4	402	70.3	295.1
ESPE-I-19	−36	289	5	4.8	−47.8	374	81.8	320.1
ESPE-I-18	−36	289	4	356.4	−55.9	908	87.1	189.3
ESPE-I-17	−36	289	4	357.3	−47.8	697	82.5	270.6
ESPE-I-16	−36	289	4	16.7	−59.0	622	76.3	40.1
ESPE-I-15	−36	289	5	10.3	−49.0	635	79.4	346.8
ESPE-I-13	−36	289	4	23.6	−44.0	191	67.4	358.8
ESPE-I-12	−36	289	3	22.5	−51.0	485	70.9	12.6
ESPE-I-11	−36	289	4	14.1	−56.3	1886	78.6	27.6
ESPE-I-10	−36	289	5	2.2	−40.5	92	77.0	298.1
ESPE-I-9′	−36	289	5	3.5	−46.3	354	81.1	309.6
ESPE-I-9	−36	289	6	358.7	−46.9	226	82.0	280.8
ESPE-I-8	−36	289	6	5.4	−40.3	675	76.2	310.4
ESPE-I-7	−36	289	5	356.3	−43.7	353	79.1	271.2
ESPE-I-6	−36	289	6	18.2	−56.4	498	75.4	28.3
ESPE-I-5	−36	289	6	5.3	−54.8	441	85.6	11.8
ESPE-I-4	−36	289	6	355.3	−54.9	361	86.1	206.2
ESPE-I-2	−36	289	6	352.7	−49.6	233	81.7	239.4
ESPE-I-1	−36	289	5	1.8	−47.4	252	82.4	301.1
ESPE-II-7	−36	289	4	343.4	−55.7	1391	76.6	193.2

Table A4. (continued)

Site Name	λ_s	ϕ_s	N_{samp}	Dec	Inc	k	λ_V	ϕ_V
ESPE-II-6	−36	289	6	352.4	−56.6	237	83.8	186.0
ESPE-II-4	−36	289	6	6.5	−57.1	308	84.5	39.1
ESPE-II-3	−36	289	5	355.9	−54.3	161	86.5	217.2
ESPE-II-2	−36	289	3	359.3	−55.0	990	89.3	238.5
ESPE-II-1	−36	289	5	1.8	−68.3	239	74.5	104.9
QTW-10-48	−36	289	5	11.5	−22.2	40	63.4	315.0
QTW-10-46	−36	289	4	10.6	−51.2	378	80.3	357.0
QTW-10-45	−36	289	5	359.2	−57.3	5162	88.0	127.4
QTW-10-44	−36	289	5	331.0	−54.7	762	66.5	192.4
QTW-10-43	−36	289	6	354.1	−55.4	596	85.2	198.2
QTW-10-42	−36	289	6	5.1	−60.8	210	83.0	76.4
QTW-10-41	−36	289	5	357.9	−55.7	454	88.3	190.4
QTW-10-40	−36	289	5	352.0	−50.8	144	82.0	230.9
QTW-10-39	−36	289	5	354.9	−52.1	854	84.7	235.6
QTW-10-38	−36	289	5	1.9	−61.9	91	82.7	98.1
QTW-10-37	−36	289	5	2.7	−52.0	471	85.9	323.3
QTW-10-36	−36	289	5	355.3	−54.6	148	86.1	210.6
QTW-10-35	−36	289	4	2.3	−50.5	1072	84.9	311.7
QTW-10-34	−36	289	5	1.8	−54.0	246	89.0	84.4
QTW-10-33	−36	289	5	1.2	−52.9	599	87.3	310.8
QTW-10-32	−36	289	6	3.9	−53.8	1217	86.4	352.7
QTW-10-30	−36	289	5	0.5	−58.1	262	87.2	101.1
QTW-10-29	−36	289	5	5.8	−55.8	470	85.3	25.0
QTW-10-28	−36	289	4	345.9	−46.4	440	75.5	229.9
QTW-10-27	−36	289	5	343.9	−50.1	176	75.6	215.4
QTW-10-26	−36	289	4	340.8	−47.2	183	72.1	218.9
QTW-10-25	−36	289	5	347.2	−49.9	305	78.1	221.8
QTW-10-24	−36	289	5	344.2	−47.7	145	74.9	223.1
QTW-10-23	−36	289	5	345.0	−49.5	693	76.3	219.1
QTW-10-22	−36	289	5	347.7	−49.5	272	78.3	224.4
QTW-10-21	−36	289	4	350.0	−49.2	806	79.7	231.5
QTW-10-20	−36	289	4	350.0	−52.3	357	81.2	216.8
QTW-10-19	−36	289	5	344.7	−43.7	762	73.2	233.5
QTW-10-18	−36	289	4	341.6	−41.7	308	70.1	231.1
QTW-10-18s	−36	289	6	324.1	−50.1	100	59.8	198.4
QTW-10-17	−36	289	3	325.6	−50.2	226	61.0	199.1
QTW-10-16	−36	289	4	355.4	−40.4	179	76.5	270.8
QTW-10-15	−36	289	5	5.6	−26.7	179	67.5	303.5
QTW-10-14	−36	289	5	359.2	−40.2	267	76.9	285.9
QTW-10-13	−36	289	4	354.9	−45.0	100	79.6	263.0
QTW-12-10	−36	289	6	337.4	−56.7	199	71.9	188.3
QTW-12-9	−36	289	6	350.4	−59.1	266	81.5	169.1
QTW-12-8	−36	289	7	333.1	−53.6	489	68.0	196.0
QTW-12-7	−36	289	6	315.8	−56.4	26	54.8	184.1
QTW-12-6	−36	289	4	345.9	−44.2	286	74.3	235.1
QTW-12-5	−36	289	7	338.7	−44.5	699	69.3	221.6
QTW-12-4	−36	289	6	336.1	−48.9	170	69.1	209.4
QTW-12-3	−36	289	6	339.7	−49.3	1313	72.1	212.3
QTW-12-2	−36	289	7	350.9	−52.9	503	82.1	215.2
QTW-12-1	−36	289	6	327.4	−53.4	200	63.3	193.9
QTW-12-0	−36	289	8	334.3	−63.9	27	68.4	164.8
QTE-2-5	−36	289	4	160.7	33.7	65	−65.5	59.9
QTE-2-4	−36	289	7	175.9	43.3	385	−78.7	89.9
QTE-2-3	−36	289	7	170.1	45.8	134	−77.8	62.6
QTE-2-2	−36	289	6	198.7	48.7	138	−73.1	182.4
QTE-2-1	−36	289	7	181.5	45.0	39	−80.5	117.3
LV-1-21	−36	289	3	8.6	−66.5	693	75.6	85.9
LV-1-20	−36	289	5	5.4	−64.5	446	78.9	89.4
LV-1-19	−36	289	4	6.4	−55.8	499	84.8	24.8
LV-1-18	−36	289	5	357.9	−55.1	277	88.3	210.7
LV-1-17	−36	289	5	353.1	−55.2	791	84.4	199.8
LV-1-16	−36	289	5	323.9	−53.5	207	60.5	192.2

Table A4. (continued)

Site Name	λ_s	ϕ_s	N_{samp}	Dec	Inc	k	λ_V	ϕ_V
LV-1-15	−36	289	5	2.1	−53.9	690	87.7	337.4
LV-1-14	−36	289	5	349.0	−49.5	371	79.2	227.6
LV-1-13	−36	289	3	8.1	−39.4	1647	74.6	318.6
LV-1-12	−36	289	3	5.5	−41.2	262	76.8	311.7
LV-1-11	−36	289	4	4.7	−38.6	512	75.2	306.4
LV-1-10	−36	289	5	8.7	−35.6	634	72.0	316.6
LV-1-9	−36	289	5	0.5	−30.2	218	70.2	290.5
LV-1-7	−36	289	4	3.9	−39.6	593	76.1	304.2
LV-1-6	−36	289	5	4.8	−29.9	1881	69.6	302.5
LV-1-5	−36	289	4	4.7	−58.3	831	85.2	59.3
LV-1-4	−36	289	4	11.3	−42.7	306	75.2	333.1
LV-1-3	−36	289	5	20.8	−55.2	331	73.2	24.4
LV-1-2	−36	289	5	14.4	−54.2	1217	78.2	17.2
LV-1-1	−36	289	5	27.7	−60.2	436	67.8	40.9
EML-1-22	−36	289	5	0.4	−26.5	27	68.0	290.2
EML-1-21	−36	289	5	359.7	−39.7	221	76.5	287.9
EML-1-20	−36	289	5	15.4	−24.2	39	62.9	323.7
EML-1-19	−36	289	5	2.5	−45.3	99	80.6	302.9
EML-1-18	−36	289	6	10.0	−35.5	283	71.4	320.0
EML-1-17	−36	289	4	349.9	−39.7	53	73.9	253.3
EML-1-16	−36	289	4	2.9	−42.8	387	78.6	302.5
EML-1-15	−36	289	4	347.6	−67.2	293	73.4	138.1
EML-1-14	−36	289	6	341.2	−51.6	169	74.0	207.3
EML-1-13	−36	289	5	347.7	−46.9	102	76.9	232.8
EML-1-12	−36	289	4	356.9	−43.5	139	79.1	274.2
EML-1-11	−36	289	5	1.8	−44.1	184	79.7	298.2
EML-1-10	−36	289	6	355.8	−55.4	166	86.6	199.0
EML-1-7	−36	289	5	336.0	−49.3	417	69.1	208.4
EML-1-6	−36	289	5	23.1	−50.0	6	70.1	10.6
EML-1-5	−36	289	5	46.2	−47.8	436	50.7	22.2
EML-1-4	−36	289	4	11.5	−59.8	135	79.9	50.0
EML-1-3	−36	289	4	11.1	−69.6	92	71.0	88.5
EML-1-0	−36	289	5	6.6	−54.5	179	84.5	10.8
QCN-1-3	−36	289	4	7.0	−40.2	593	75.6	315.9
QCN-1-2	−36	289	5	2.7	−53.7	858	87.2	341.4
QCN-1-1	−36	289	5	28.2	−67.9	179	64.9	64.5
QC-1	−36	289	4	317.6	−66.3	118	56.7	163.3

[a] Definitions are as follows: λ_s, site latitude; ϕ_s, site longitude; N_{samp}, number of samples at the site; k, estimated Fisherian precision parameter; λ_V, VGP latitude; ϕ_V, VGP longitude.

A4. Tatara San Pedro, Chile

[54] Tatara San Pedro, Chile, is an eruptive complex of the volcanic front of the Andean southern volcanic zone, with at least three central vent regions. Quaternary volcanism began about 930 ka, and both mafic and silicic lavas are present. The geology and chronology of the region is described in detail by *Singer et al.* [1997]. Paleomagnetic data were collected over several field seasons by L. Brown, B. Singer and colleagues and directional data from 193 sites are available for our study. K-Ar radiometric ages are available for 22 of these sites [*Singer et al.*, 1997, Table 1], with one site having both a K-Ar and Ar-Ar [*Singer et al.*, 1997, Table 2] age. Paleomagnetic data are from the following sections: Estero Molino, Estero Pellado, Estero San Pedro, Quebrada Turbia and Laguna Verde. The Matuyama-Brunhes transition is recorded in two sections of the Quebrada Turbia sequence, and paleomagnetic data from 32 sites from these sections is reported by *Brown et al.* [2004b]. Data from the additional 161 sites are given in Table A4.

Acknowledgments

[55] This work was supported under NSF grants EAR-9805164 (Tauxe), EAR-0337712 (C. Johnson, C. Constable), EAR-0516760, EAR-0337684, EAR-9909309 (B. Singer), EAR-0608998 and EAR-0229130 (N. Opdyke), EAR-9870309 and EAR-9943700 (D. Stone and P. Layer), and EAR-04400018 (L. Brown), and by NSERC (R. Barendregt).

C. Johnson acknowledges the Institut de Physique du Globe de Paris for support as a visiting researcher during preparation of this manuscript. We thank Kristin Lawrence for input on the 20° latitude regional compilation. Comments by J. Tarduno and reviews from R. Van der Voo, J.-P. Valet, and an anonymous reviewer are much appreciated.

References

Bloxham, J., and A. Jackson (1992), Time-dependent mapping of the magnetic field at the core-mantle boundary, *J. Geophys. Res.*, *97*, 19,537–19,563.

Bloxham, J., D. Gubbins, and A. Jackson (1989), Geomagnetic secular variation, *Philos. Trans. R. Soc., Ser. A*, *329*, 415–502.

Bouligand, C., G. Hulot, A. Khokhlov, and G. A. Glatzmaier (2005), Statistical paleomagnetic field modelling and dynamo numerical simulation, *Geophys. J. Int.*, *161*, 603–626.

Briggs, R. M., T. Okada, T. Itaya, H. Shibuya, and I. E. M. Smith (1994), K-Ar ages, paleomagnetism, and geochemistry of the South Auckland volcanic field, North Island, New Zealand, *N. Z. J. Geol. Geophys.*, *37*, 143–153.

Brown, L. (2002), Paleosecular variation from Easter Island revisited: Modern demagnetization of a 1970s data set, *Phys. Earth Planet. Inter.*, *133*, 73–81.

Brown, L. L., B. S. Singer, and M. Gorring (2004a), Paleomagnetism and $^{40}Ar/^{39}Ar$ chronology of lavas from Meseta del Lago Buenos Aires, Patagonia, *Geochem. Geophys. Geosyst.*, *5*, Q01H04, doi:10.1029/2003GC000526.

Brown, L. L., B. S. Singer, J. C. Pickens, and B. R. Jicha (2004b), Paleomagnetic directions and $^{40}Ar/^{39}Ar$ ages from the Tatara San Pedro volcanic complex, Chilean Andes: Lava record of a Matuyama-Brunhes precursor?, *J. Geophys. Res.*, *109*, B12101, doi:10.1029/2004JB003007.

Carlut, J., and V. Courtillot (1998), How complex is the time-averaged geomagnetic field over the last 5 million years?, *Geophys. J. Int.*, *134*, 527–544.

Christensen, U. R., and P. Olson (2003), Secular variaiton in numerical geodynamo models with lateral variations of boundary heat flow, *Phys. Earth Planet. Inter.*, *138*, 39–54.

Coe, R. S., X. Zhao, J. J. Lyons, C. J. Pluhar, and E. A. Mankinen (2000), Revisiting the 1964 collection of Nunivak lava flows, *Eos Trans. AGU*, *81*(48), Fall Meeting Suppl., Abstract GP62A-06.

Constable, C. G. (2007), Centennial to millennial-scale geomagnetic field variations, in *Treatise on Geophysics*, vol. 5, *Geomagnetism*, edited by M. Kono, chap. 9, Elsevier, New York.

Constable, C. G., and C. L. Johnson (1999), Anisotropic paleosecular variation models: Implications for geomagnetic observables, *Phys. Earth Planet. Inter.*, *115*, 35–51.

Constable, C. G., and R. L. Parker (1988), Statistics of the geomagnetic secular variation for the past 5 m.y., *J. Geophys. Res.*, *93*, 11,569–11,581.

Cox, A. (1969), A paleomagnetic study of secular variation in New Zealand, *Earth Planet. Sci. Lett.*, *6*, 257–267.

Cox, A. (1971), Remanent magnetization and susceptibility of late Cenozoic rocks from New Zealand, *N. Z. J. Geol. Geophys.*, *14*, 192–207.

Creer, K. M. (1962), The dispersion of the geomagnetic field due to secular variation and its determination from remote times from paleomagnetic data, *J. Geophys. Res.*, *67*, 3461–3476.

Creer, K. M. (1983), Computer synthesis of geomagnetic paleosecular variations, *Nature*, *304*, 695–699.

DeMets, C., R. G. Gordon, D. F. Argus, and S. Stein (1994), Effect of recent revisions to the geomagnetic reversal time scale on estimates of current plate motions, *Geophys. Res. Lett.*, *21*, 2191–2194.

Glatzmaier, G. A., R. S. Coe, L. Hongre, and P. H. Roberts (1999), The role of the Earth's mantle in controlling the frequency of geomagnetic reversals, *Nature*, *401*, 885–890.

Gubbins, D., and P. Kelly (1993), Persistent patterns in the geomagnetic field over the past 2.5 Myr, *Nature*, *365*, 829–832.

Heki, K. (1983), Paleomagnetic study of the Higashi-Izu Volcano Group and pyroclastics flow deposits in Kagoshima Prefecture: Paleosecular variation during the last 40,000 years, *J. Geomagn. Geoelectr.*, *35*, 383–390.

Hollerbach, R., and C. Jones (1993a), A geodynamo model incorporating a finitely conducting inner core, *Phys. Earth Planet. Inter.*, *75*, 317–327.

Hollerbach, R., and C. Jones (1993b), Influence of Earth's inner core on geomagnetic fluctutations and reversals, *Nature*, *365*, 541–543.

Hongre, L., G. Hulot, and A. Khokhlov (1998), An analysis of the geomagnetic field over the past 2000 years, *Phys. Earth Planet. Inter.*, *106*, 311–335.

Hulot, G., C. Eymin, B. Langlais, M. Mandea, and N. Olsen (2002), Small-scale structure of the geodynamo inferred from Oersted and Magsat satellite data, *Nature*, *416*, 620–623.

Ishikawa, N., and T. Tagami (1991), Paleomagnetism and fission-track geochronology on the Goto and Tsushima Islands in the Tsushima Strait area: Implications for the opening mode of the Japan Sea, *J. Geomagn. Geoelectr.*, *43*, 229–253.

Jackson, A., A. R. T. Jonkers, and M. R. Walker (2000), Four centuries of geomagnetic secular variation from historical records, *Philos. Trans. R. Soc., Ser. A*, *358*, 957–990.

Johnson, C. L., and C. G. Constable (1995), The time-averaged geomagnetic field as recorded by lava flows over the past 5 Myr, *Geophys. J. Int.*, *122*, 489–519.

Johnson, C. L., and C. G. Constable (1996), Paleosecular variation recorded by lava flows over the last 5 Myr, *Philos. Trans. R. Soc., Ser. A*, *354*, 89–141.

Johnson, C. L., and C. G. Constable (1997), The time-averaged geomagnetic field: Global and regional biases for 0–5 Ma, *Geophys. J. Int.*, *131*, 643–666.

Johnson, C. L., and P. McFadden (1997), The time-averaged field and paleosecular variation, in *Treatise on Geophysics*, vol. 5, *Geomagnetism*, edited by M. Kono, chap. 11, Elsevier, New York.

Johnson, C. L., J. R. Wijbrans, C. G. Constable, J. Gee, H. Staudigel, L. Tauxe, V.-H. Forjaz, and M. Salgueiro (1998), $^{40}Ar/^{39}Ar$ ages and paleomagnetism of São Miguel lavas, Azores, *Earth Planet. Sci. Lett.*, *160*, 637–649.

Kelly, P., and D. Gubbins (1997), The geomagnetic field over the past 5 Myr, *Geophys. J. Int.*, *128*, 315–330.

Kent, D. V., and M. A. Smethurst (1998), Shallow bias of inclinations in the Paleozoic and Precambrian, *Earth Planet. Sci. Lett.*, *160*, 391–402.

Khokhlov, A., G. Hulot, and J. Carlut (2001), Towards a self-consistent approach to palaeomagnetic field modelling, *Geophys. J. Int.*, *145*, 157–171.

Khokhlov, A., G. Hulot, and C. Bouligand (2006), Testing statistical palaeomagnetic field models against directional data affected by measurement errors, *Geophys. J. Int.*, *167*, 635–648.

Kikawa, E., M. Koyama, and H. Kinoshita (1989), Paleomagnetism of Quaternary volcanics in the Izu Peninsula and adjacent areas, Japan, and its tectonic significance, *J. Geomagn. Geoelectr.*, *41*, 175–201.

Kono, M. (1968), Paleomagnetism of Pleistocene Usami Volcano, Izu Peninsula, Japan—Intensity of the Earth's magnetic field in geological time II, *J. Geomagn. Geoelectr.*, *20*, 353–366.

Kono, M. (1971), Intensity of the Earth's magnetic field in geological time III. Pleistocene and Pliocene data from Japanese volcanic rocks, *J. Geomagn. Geoelectr.*, *23*, 1–9.

Kono, M., and P. H. Roberts (2002), Recent geodynamo simulations and observations of the geomagnetic field, *Rev. Geophys.*, *40*(4), 1013, doi:10.1029/2000RG000102.

Korte, M., and C. G. Constable (2005), Continuous geomagnetic models for the past 7 millennia: 2. CALS7K, *Geochem. Geophys. Geosyst.*, *6*, Q02H16, doi:10.1029/2004GC000801.

Lawrence, K., C. G. Constable, and C. L. Johnson (2006), Paleosecular Variation and the average geomagnetic field at ±20° latitude, *Geochem. Geophys. Geosyst.*, *7*, Q07007, doi:10.1029/2005GC001181.

Lee, S. (1983), A study of the time-averaged paleomagnetic field for the past 195 million years, Ph.D. thesis, Aust. Natl. Univ., Canberra, ACT, Australia.

McElhinny, M. W., and P. L. McFadden (1997), Palaeosecular variation over the past 5 Myr based on a new generalized database, *Geophys. J. Int.*, *131*, 240–252.

McElhinny, M. W., and R. T. Merrill (1975), Geomagnetic secular variation over the past 5 my, *Rev. Geophys.*, *13*, 687–708.

McElhinny, M. W., P. L. McFadden, and R. T. Merrill (1996), The time-averaged paleomagnetic field 0–5 Ma, *J. Geophys. Res.*, *101*, 25,007–25,027.

McFadden, P. L. (2004), Is 600 Myr long enough for the random paleogeographic test of the geomagnetic axial dipole assumption?, *Geophys. J. Int.*, *158*, 443–445.

McFadden, P. L., R. T. Merrill, and M. W. McElhinny (1988), Dipole/quadrupole family modelling of paleosecular variation, *J. Geophys. Res.*, *93*, 11,583–11,588.

Mejia, V., R. W. Barendregt, and N. D. Opdyke (2002), Paleosecular variation of brunhes age lava flows from British Columbia, Canada, *Geochem. Geophys. Geosyst.*, *3*(12), 8801, doi:10.1029/2002GC000353.

Mejia, V., N. D. Opdyke, J. F. Vilas, B. S. Singer, and J. S. Stoner (2004), Plio-Pleistocene time-averaged field in southern Patagonia recorded in lava flows, *Geochem. Geophys. Geosyst.*, *5*, Q03H08, doi:10.1029/2003GC000633.

Mejia, V., H. Böhnel, N. D. Opdyke, M. A. Otega-Rivera, J. K. W. Lee, and J. J. Aranda-Gomez (2005), Paleosecular variation and time-averaged field recorded in late Pliocene–Holocene lava flows from Mexico, *Geochem. Geophys. Geosyst.*, *6*, Q07H19, doi:10.1029/2004GC000871.

Merrill, R. T., M. W. McElhinny, and P. L. McFadden (1996), *The Magnetic Field of the Earth: Paleomagnetism, the Core and the Deep Mantle*, Academic Press, San Diego, Calif.

Olson, P., and J. Aurnou (1999), A polar vortex in the Earth's core, *Nature*, *402*, 170–173.

Opdyke, N., and R. Musgrave (2004), Paleomagnetic results from the Newer Volcanics of Victoria: Contribution to the Time Averaged Field Initiative, *Geochem. Geophys. Geosyst.*, *5*, Q03H09, doi:10.1029/2003GC000632.

Opdyke, N. D., M. Hall, V. Mejia, K. Huang, and D. A. Foster (2006), The time-averaged field at Ecuador: Results from the equator, *Geochem. Geophys. Geosyst.*, *7*, Q11005, doi:10.1029/2005GC001221.

Otake, H., H. Tanaka, M. Kono, and K. Saito (1993), Paleomagnetic study of Pleistocene lavas and dikes of the Zao Volcanic Group, Japan, *J. Geomagn. Geoelectr.*, *45*, 595–612.

Parker, R. L. (1994), *Geophysical Inverse Theory*, Princeton Univ. Press, Princeton, N. J.

Piper, J. D. A., and S. Grant (1989), A paleomagnetic test of the axial dipole assumption and implications for continental distributions through geological time, *Phys. Earth Planet. Inter.*, *55*, 37–53.

Quidelleur, X., et al. (1994), Long-term geometry of the geomagnetic field for the last 5 million years: An updated secular variation database from volcanic sequences, *Geophys. Res. Lett.*, *21*, 1639–1642.

Schneider, D. A., and D. V. Kent (1990), The time-averaged paleomagnetic field, *Rev. Geophys.*, *28*, 71–96.

Shane, P., T. Black, and J. Westgate (1994), Isothermal plateau fission-track age for a paleomagnetic excursion in the Mamaku Ignimbrite, New Zealand, and implications for late Quaternary stratigraphy, *Geophys. Res. Lett.*, *21*, 1695–1698.

Shibuya, H., J. Cassidy, I. E. M. Smith, and T. Itaya (1992), A geomagnetic excursion in the Brunhes chron recorded in New Zealand basalts, *Earth Planet. Sci. Lett.*, *111*, 41–48.

Shibuya, H., J. Cassidy, I. E. M. Smith, and T. Itaya (1995), Paleomagnetism of young New Zealand basalts and longitudinal distribution of paleosecular variation, *J. Geomagn. Geoelectr.*, *47*, 1011–1022.

Singer, B. S., R. A. Thompson, M. A. Dungan, T. C. Feeley, S. T. Nelson, J. C. Pickens, L. L. Brown, A. W. Wulff, J. P. Davidson, and J. Metzger (1997), Volcanism and erosion during the past 930 k.y. at the Tatara San Pedro complex, Chilean Andes, *GSA Bull.*, *109*, 127–142.

Solheid, P., C. Constable, A. Koppers, M. Jackson, and S. Banerjee (2002), Research-oriented data base for rock and paleomagnetism to be developed, *Eos Trans. AGU*, *83*(48), 560.

Sreenivasan, B., and C. A. Jones (2005), Structure and dynamics of the polar vortex in the Earth's core, *Geophys. Res. Lett.*, *32*, L20301, doi:10.1029/2005GL023841.

Sreenivasan, B., and C. A. Jones (2006), Azimuthal winds, convection and dynamo action in the polar region of the planetary cores, *Geophys. Astrophys. Fluid Dyn.*, *100*, 319–339.

Stone, D. B., and P. W. Layer (2006), Paleosecular variation and GAD studies of 0_2 Ma flow sequences from the Aleutian Islands, Alaska, *Geochem. Geophys. Geosyst.*, *7*, Q04H22, doi:10.1029/2005GC001007.

Tanaka, H. (1990), Paleointensity high at 9000 years ago from volcanic rocks in Japan, *J. Geophys. Res.*, *95*, 17,517–17,531.

Tanaka, H., and T. Kobayashi (2003), Paleomagnetism of the late Quaternary Ontake Volcano, Japan: Directions, intensities, and excursions, *Earth Planets Space*, *55*, 189–202.

Tanaka, H., A. Otsuka, T. Tachibana, and M. Kono (1994), Paleointensities for 10–22 ka from volcanic rocks in Japan and New Zealand, *Earth Planet. Sci. Lett.*, *122*, 29–42.

Tanaka, H., G. M. Turner, B. F. Houghton, T. Tachibana, M. Kono, and M. O. McWilliams (1996), Palaeomagnetism and chronology of the central Taupo Volcanic Zone, *Geophys. J. Int.*, *124*, 919–934.

Tanaka, H., K. Kawamura, K. Nagao, and B. F. Houghton (1997), K-Ar ages and paleosecular variation of direction and intensity from Quaternary lava sequences in the Ruapehu Volcano, New Zealand, *J. Geomagn. Geoelectr.*, *49*, 587–599.

Tauxe, L., and D. Kent (2004), A simplified statistical model for the geomagnetic field and the detection of shallow bias in paleomagnetic inclinations: Was the ancient magnetic field dipolar?, in *Timescales of the Internal Geomagnetic Field*, *Geophys. Monogr. Ser.*, vol. 145, edited by J. E. T. C. Channell et al., pp. 101–115, AGU, Washington, D. C.

Tauxe, L., and T. Yamazaki (2007), Paleointensities, in *Treatise on Geophysics*, *Geomagnetism*, edited by M. Kono, chap. 13, Elsevier, New York.

Tauxe, L., H. Staudigel, and J. Wijbrans (2000), Paleomagnetism and $^{40}Ar/^{39}Ar$ ages from La Palma in the Canary Islands, *Geochem. Geophys. Geosyst.*, *1*(9), doi:10.1029/2000GC000063.

Tauxe, L., C. Constable, C. L. Johnson, A. A. P. Koppers, W. R. Miller, and H. Staudigel (2003), Paleomagnetism of the southwestern U.S.A. recorded by 0–5 Ma igneous rocks, *Geochem. Geophys. Geosyst.*, *4*(4), 8802, doi:10.1029/2002GC000343.

Tauxe, L., P. Gans, and E. A. Mankinen (2004a), Paleomagnetism and 40Ar/39Ar ages from volcanics extruded during the Matuyama and Brunhes Chrons near McMurdo Sound, Antarctica, *Geochem. Geophys. Geosyst.*, *5*, Q06H12, doi:10.1029/2003GC000656.

Tauxe, L., C. Luskin, P. Selkin, P. Gans, and A. Calvert (2004b), Paleomagnetic results from the Snake River Plain: Contribution to the time-averaged field global database, *Geochem. Geophys. Geosyst.*, *5*, Q08H13, doi:10.1029/2003GC000661.

Torsvik, T. H., and R. Van der Voo (2002), Refining Gondwana and Pangea paloegeography: Estimates of Phanerozoic non-dipole (octupole) fields, *Geophys. J. Int.*, *151*, 771–794.

Tsunakawa, H., and Y. Hamano (1988), Paleomagnetic study of the Ashitaka Dike Swarm in central Japan, *J. Geomagn. Geoelectr.*, *40*, 221–226.

Valet, J. P., L. Meynadier, and Y. Guyodo (2005), Geomagnetic dipole strength and reversal rate over the past two million years, *Nature*, *435*, 802–805.

Vandamme, D. (1994), A new method to determine paleosecular variation, *Phys. Earth Planet. Inter.*, *85*, 131–142.

Van der Voo, R., and T. H. Torsvik (2001), Evidencefor late Paleozoic and Mesozoic non-dipole fields provides an explanation for the Pangea reconstruction problems, *Earth Planet. Sci. Lett.*, *187*, 71–81.

Wilson, R. L. (1970), Permanent aspects of the Earth's non-dipole magnetic field over Upper Tertiary times, *Geophys. J. R. Astron. Soc.*, *19*, 417–439.